miRNA-203b-3p Induces Acute and Chronic Pruritus through 5-HTR2B and TRPV4

JID Open

Francesco De Logu[1], Roberto Maglie[2], Mustafa Titiz[1], Giulio Poli[3], Lorenzo Landini[1], Matilde Marini[1], Daniel Souza Monteiro de Araujo[1], Gaetano De Siena[1], Marco Montini[4], Daniela Almeida Cabrini[5], Michel Fleith Otuki[5], Priscila Lúcia Pawloski[5], Emiliano Antiga[2], Tiziano Tuccinardi[3], João Batista Calixto[6], Pierangelo Geppetti[5], Romina Nassini[1] and Eunice André[5]

Growing evidence indicates that transient receptor potential (TRP) channels contribute to different forms of pruritus. However, the endogenous mediators that cause itch through transient receptor potential channels signaling are poorly understood. In this study, we show that genetic deletion or pharmacological antagonism of TRPV4 attenuated itch in a mouse model of psoriasis induced by topical application of imiquimod. Human psoriatic lesions showed increased expression of several microRNAs, including the miR-203b-3p, which induced a calcium ion response in rodent dorsal root ganglion neurons and scratching behavior in mice through 5-HTR2B activation and the protein kinase C–dependent phosphorylation of TRPV4. Computer simulation revealed that the miR-203b-3p core sequence (GUUAAGAA) that causes 5-HTR2B/TRPV4-dependent itch targets the extracellular side of 5-HTR2B by interacting with a portion of the receptor pocket consistent with its activation. Overall, we reveal the unconventional pathophysiological role of an extracellular microRNA that can behave as an itch promoter through 5-HTR2B and TRPV4.

Journal of Investigative Dermatology (2023) **143,** 142–153; doi:10.1016/j.jid.2022.08.034

INTRODUCTION

Pruritus is an unpleasant sensation, that is, an itch, which leads to the urge to scratch and generally accompanies inflammatory skin diseases. Occasionally, chronic pruritus occurs during the progression of systemic diseases, including liver and renal diseases and various malignancies, significantly impacting patient QOL (Hashimoto and Yosipovitch, 2019). A subgroup of nonselective calcium ion (Ca^{2+}) permeable cation channels, predominantly expressed in a subpopulation of the C- or Aδ-fibers of dorsal root ganglia (DRG) neurons, have received growing interest in a number of physiological and pathophysiological processes, including itch (Caterina and Pang, 2016; Wei et al., 2020; Wilson et al., 2013, 2011). Namely, TRPV1 and TRPV4 and TRPA1 are of specific interest regarding itch. For example, TRPV1 and TRPA1 are implicated in signaling the acute and chronic itch evoked by histaminergic and nonhistaminergic stimuli (Croce and Calin, 2005; Maglie et al., 2021; Wilson et al., 2011; Xie and Hu, 2018). It has also been reported that TRPV4 can mediate serotonin (5-HT)–induced itch because around 90% of sensory neurons that respond to 5-HT express TRPV4, and the neuronal response to 5-HT stimulation was reduced by TRPV4 genetic deletion (Akiyama et al., 2016; Snyder et al., 2016).

MicroRNAs (miRNAs) are short, single-stranded, noncoding RNA molecules that are increasingly being investigated for their ability to regulate gene expression by binding to the 3′ untranslated regions of cytosolic mRNA targets (Hayes et al., 2014). Recently, an unconventional signaling role of miRNA in itch was identified using a mouse model of cutaneous T-cell lymphoma. Specifically, extracellular miR-711 produced by neoplastic cells promoted a scratching behavior by directly gating the TRPA1 channel (Han et al., 2018). More recently, a miR-146a was identified as a key signaling molecule in cholestatic itch and is released from keratinocytes (KCs) after TRPV4 stimulation by lysophosphatidylcholine, a precursor of the lysophosphatidic acid (Chen et al., 2021).

We hypothesized that in addition to cancer and cholestatic pruritus, miRNA dysregulation is mechanistically implicated in itch associated with inflammatory skin diseases. For example, the miRNA signature of psoriasis in skin biopsies has revealed the upregulation of a series of miRNAs, including miR-203, miR-184, miR-135b, miR-142-3p, miR-21, and miR-31 (Domingo et al., 2020; Timis and Orasan, 2018). Therefore, we explored which of these miRNAs could mediate itch in a mouse model of psoriasis. Specifically, we found that miR-203b-3p, a KC-derived miRNA, was able to directly elicit itch in wild-type mice and was critical for itch induction in psoriatic mice through the activation of the 5-HTR2B/TRPV4 neuronal pathway.

[1]*Section of Clinical Pharmacology and Oncology, Department of Health Sciences, University of Florence, Florence, Italy;* [2]*Section of Dermatology, Department of Health Sciences, University of Florence, Florence, Italy;* [3]*Department of Pharmacy, University of Pisa, Pisa, Italy;* [4]*Medical Genetics Unit, Department of Experimental and Clinical Biomedical Sciences "Mario Serio", University of Florence, Florence, Italy;* [5]*Department of Pharmacology, Federal University of Paraná, Curitiba, Brazil; and* [6]*Centro de Inovação e Ensaios Pré-Clínicos (CIEnP), Florianópolis, Brazil*

Correspondence: Romina Nassini, Section of Clinical Pharmacology and Oncology, Department of Health Sciences, University of Florence, Viale Pieraccini, Florence 650139, Italy. E-mail: romina.nassini@unifi.it

Abbreviations: 5-HT, serotonin; Ca^{2+}, calcium ion; DRG, dorsal root ganglia; GSK, GSK-1016790A; HC-06, HC067047; HEK, human embryonic kidney; IMQ, imiquimod; KC, keratinocyte; MD, molecular dynamics; miRNA, MicroRNA; PKC, protein kinase C

Received 9 March 2022; revised 17 June 2022; accepted 5 August 2022; accepted manuscript published online 30 August 2022; corrected proof published online 8 October 2022

RESULTS

Trpv4 genetic deletion protects from miRNA-203b-3p–induced scratching behavior in mice

A search for miRNAs that are dysregulated in patients with psoriasis revealed that some miRNAs were upregulated in skin biopsies from patients with psoriasis (Domingo et al., 2020). Thus, we tested whether the corresponding mouse miRNA isoforms were capable of provoking a scratching behavior in naive mice after subcutaneous injection in the nape of the neck. Among the eight mouse miRNAs tested (mmu-miR-203b-3p, mmu-miR-203a-5p, mmu-miR-146-5p, mmu-miR-146-3p, mmu-miR-31-3p, mmu-miR-31-5p, mmu-miR-21-3p, and mmu-miR-21-5p), only mmu-miR-203b-3p elicited a dose-dependent scratching behavior in naive mice (Figure 1a and b). In addition, using a check model to distinguish itch from pain (Shimada and LaMotte, 2008), we showed that mmu-miR-203b-3p failed to evoke any measurable nociceptive behavior (wiping) at all tested doses (Figure 1b). Because TRPA1, TRPV1, and TRPV4 channels expressed by pruriceptive DRG neurons are implicated in either acute or chronic pruritus (Sun and Dong, 2016), we explored whether mmu-miR-203b-3p triggers the scratching behavior through the activation of transient receptor potential channels. Subcutaneous injection of mmu-miR-203b-3p induced a scratching behavior in *Trpa1*$^{-/-}$ and *Trpv1*$^{-/-}$ similar to the behavior observed in their wildtype littermates (Fig. 1c). However, mmu-miR-203b-3p-induced scratching behavior was absent in *Trpv4*$^{-/-}$ mice (Figure 1c). As previously reported (Kittaka et al., 2017), we confirm that a TRPV4 agonist, GSK-1016790A (GSK), provoked a dose-dependent scratching behavior in mice, which was attenuated in mice treated with a TRPV4 antagonist, HC067047 (HC-06) (Supplementary Figure S1a), and in *Trpv4*$^{-/-}$ mice (Supplementary Figure S1b). Moreover, HC-06 attenuated the scratching behavior elicited by mmu-miR-203b-3p (Supplementary Figure S1c).

miR-203b-3p indirectly targets the TRPV4 channel through 5-HTR2B

We next tested whether miR-203b-3p directly gated TRPV4 channels by analyzing the Ca^{2+} response in human TRPV4–human embryonic kidney (HEK) 293 and mouse TRPV4–HEK293 cells. Although GSK elicited a robust Ca^{2+} response that could be abolished by HC-06, the (human) hsa-miR-203b-3p and mmu-miR-203b-3p failed to elicit any response (Figure 2a and Supplementary Figure S1d). Moreover, hsa-miR-203b-3p failed to evoke any Ca^{2+} response in human TRPV1–HEK293 and human TRPA1–HEK293 cells (Supplementary Figure S1e and f).

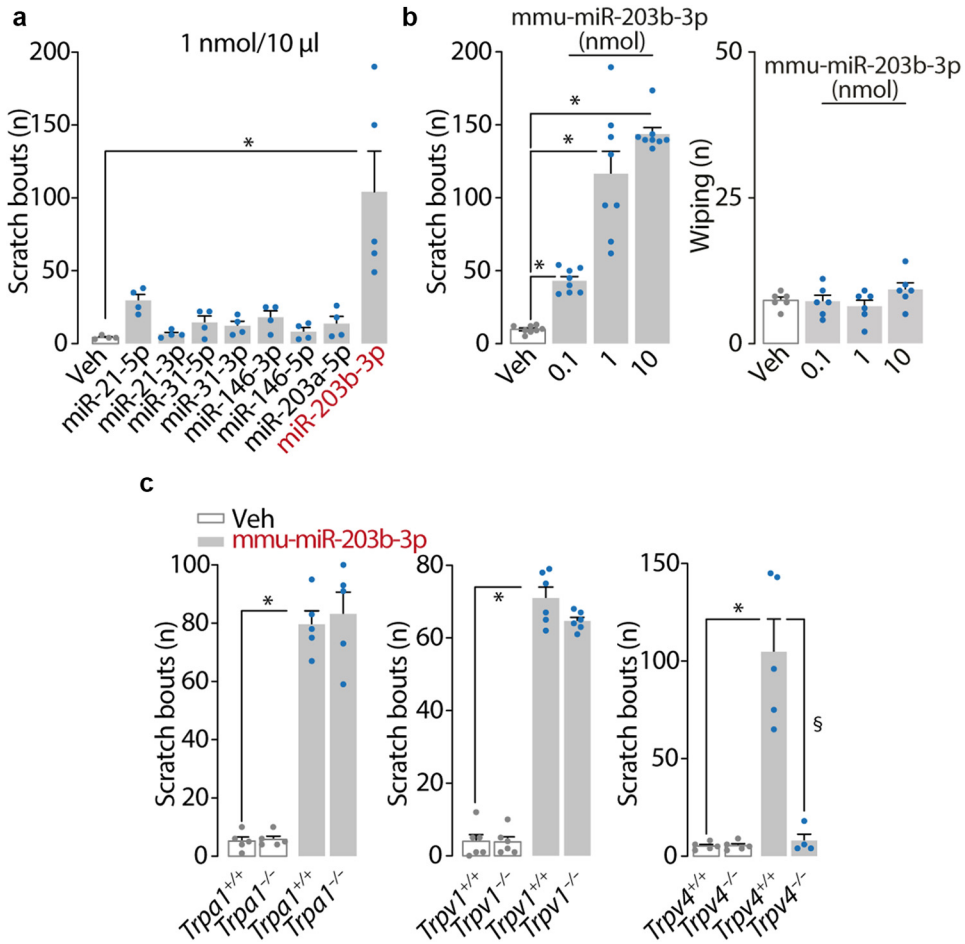

Figure 1. Intradermal miR-203b-3p induces scratching behavior through TRPV4. (**a**) Scratching behavior in C57BL/6J mice was induced by i.d. (10 µl) injection of mmu-miR-203b-3p but not by mmu-miR-203a-5p, mmu-miR-146-5p, mmu-miR-146-3p, mmu-miR-31-3p, mmu-miR-31-5p, mmu-miR-21-3p, and mmu-miR-21-5p (1 nmol for all) or Veh. (**b**) Dose-dependent scratching behavior and wiping in C57BL/6J mice induced by mmu-miR-203b-3p (0.1–10 nmol, i.d.) or Veh. (**c**) Scratching behavior in *Trpa1*$^{+/+}$ and *Trpa1*$^{-/-}$, *Trpv1*$^{+/+}$ and *Trpv1*$^{-/-}$, or *Trpv4*$^{+/+}$ and *Trpv4*$^{-/-}$ mice induced by mmu-miR-203b-3p (1 nmol, i.d.) or Veh. Data are presented as mean ± SEM. n = 4–8 mice per group. $^{*}P < 0.05$ versus Veh, $^{§}P < 0.05$ versus mmu-miR-203b-3p. Data were analyzed with one-way ANOVA with Bonferroni correction. i.d., intradermal; Veh, vehicle.

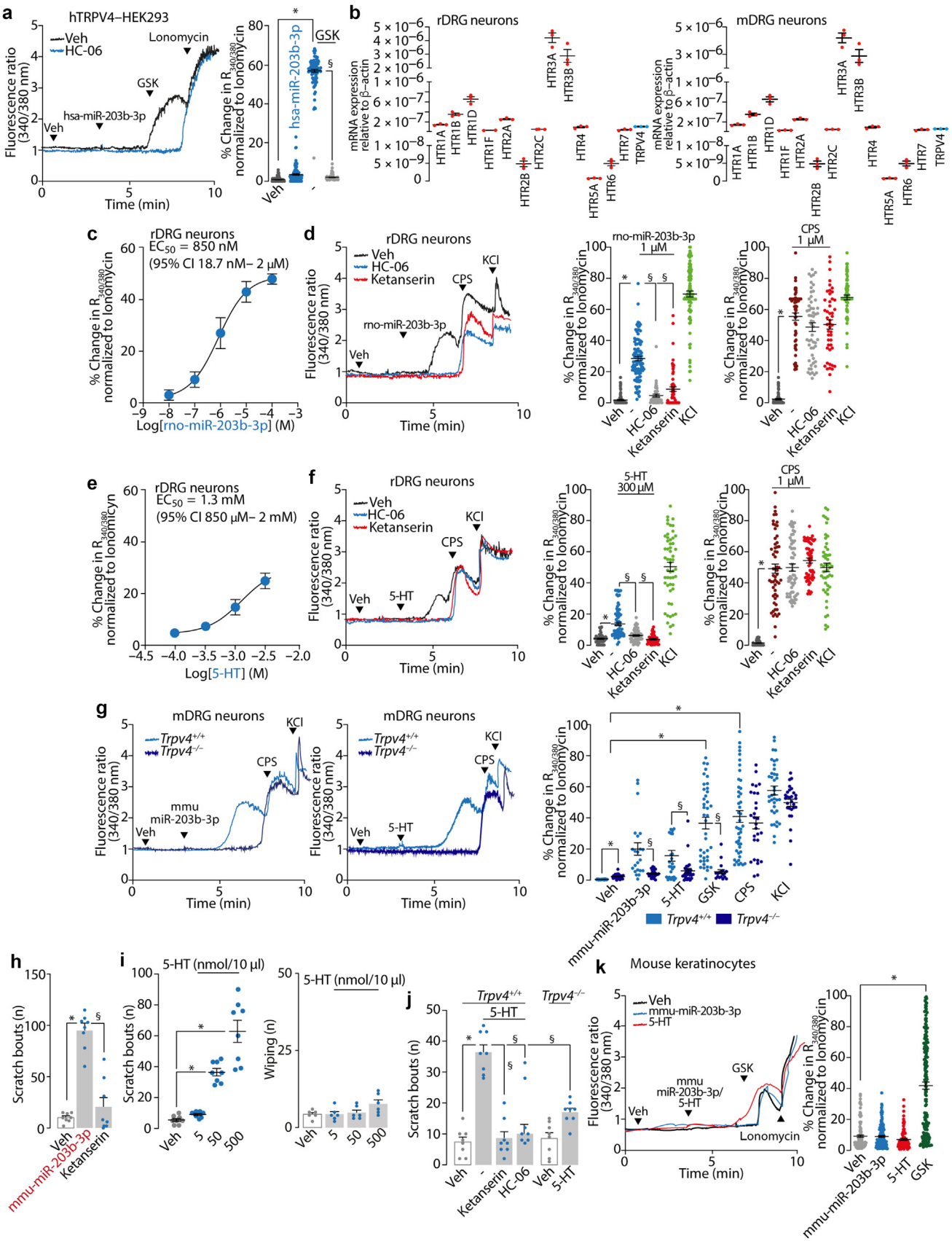

Figure 2. miR-203b-3p induces TRPV4 activation through 5-HTR2B. (**a**) Typical tracings and cumulative data of the Ca^{2+} response in hTRPV4–HEK293 cells exposed to hsa-miR-203b-3p (10 μM) and GSK (10 nM) or Veh in the presence of HC-06 (30 μM) or Veh (n = 4 independent experiments). (**b**) mRNA expression of 5-HTR and *Trpv4* in rat and mouse DRG neurons (n = 3 independent experiments). Concentration–response curve of the Ca^{2+} response to (**c**) rno-miR-203b-3p and (**e**) 5-HT in rat DRG neurons. Typical tracings and cumulative data of the Ca^{2+} response in rat DRG neurons exposed to (**d**) rno-miR-203b-3p (10 μM) or

TRPV4 is considered a key downstream component of 5-HT–induced itch (Akiyama et al., 2016), and 5-HTRs were previously shown to induce itch by coupling to TRPV4 channels (Snyder et al., 2016). We confirmed the mRNA expression of various 5-HTR subtypes (Ohta et al., 2006; Usoskin et al., 2015) and *Trpv4* in rat and mouse DRG neurons (De Logu et al., 2020) (Figure 2b). Moreover, we showed that the rat isoform of miR-203b-3p (rno-miR-203b-3p) induced a concentration-dependent Ca^{2+} response in rat DRGs neurons (Figure 2c), which was reduced by HC-06 (Figure 2d). The role of 5-HTR2B was supported by the ability of the selective receptor blocker, ketanserin, to attenuate the rno-miR-203b-3p–induced Ca^{2+} response in rat DRGs neurons (Figure 2d). The 5-HT also elicited a concentration-dependent Ca^{2+} response (Figure 2e) that was reduced by ketanserin and HC-06 (Figure 2f). Importantly, HC-06 and ketanserin did not affect the Ca^{2+} response to capsaicin (Figure 2 and f). The cooperation between 5-HTR2B and TRPV4 was further supported by the failure of mmu-miR-203b-3p, 5-HT, and GSK to evoke a Ca^{2+} response in *Trpv4*$^{-/-}$ mouse DRG neurons (Figure 2g).

Ketanserin inhibited mmu-miR-203b-3p–induced scratching behavior in vivo but did not inhibit GSK-induced scratching behavior (Figure 2h and Supplementary Figure S1g). The 5-HT injection caused a dose-dependent scratching behavior (but no wiping behavior) (Figure 2i), which was attenuated in mice pretreated with both ketanserin and HC-06 and was absent in *Trpv4*$^{-/-}$ mice (Figure 2j). To exclude the possible role of skin KCs in mmu-miR-203b-3p–induced itch, we tested the Ca^{2+} response induced by mmu-miR-203b-3p in cultured mouse epidermal KCs isolated from the skin of the back of mice. GSK elicited Ca^{2+} responses, but mmu-miR-203b-3p and 5-HT did not (Figure 2k). Collectively, these findings confirmed the expression of a functional TRPV4 channel in KCs and the absence of the 5-HTR2B that would enable these cells to respond to mmu-miR-203b-3p.

miRNA-203b-3p evokes scratching behavior through a conserved eight nucleotide itching sequence

To determine the specific sequence of miR-203b-3p responsible for the scratching behavior, we generated six sequence variants of mmu-miR-203b-3p (m1–6) by converting several nucleotides to adenosine (Figure 3a). These sequence variants were then injected subcutaneously to test their ability to induce a scratching behavior. The observation that sequence variants of four nucleotides in m3 and m4 resulted in a markedly reduced effect led us to identify GUCAAGAA as the itching core sequence of mmu-miRNA-203b-3p (Figure 3b).

A comparison of the mmu-, rno-, and hsa-miR-203b-3p sequences revealed that rno- and hsa-miR-203b-3p contain the same GUUAAGAA core sequence, whereas the mmu sequence has a cytosine instead of the second uracil. Interestingly, miR-203b-3p from the three species conserved the nucleotide sequence needed to evoke the scratching behavior (Figure 3c). Specifically, the mouse GUCAAGAA core sequence induced a scratching behavior that was attenuated by HC-06 or ketanserin and in *Trpv4*$^{-/-}$ mice (Figure 3d and e). The m1, m2, m5, and m6 core sequences but not the m3 and m4 sequences evoked a Ca^{2+} response in mouse DRG neurons (Figure 2f). The core sequence as well as GSK also induced a Ca^{2+} response in *Trpv4*$^{+/+}$ DRGs neurons that are absent in *Trpv4*$^{-/-}$ mice (Figure 3g).

miR-203b-3p activates mouse 5-HTR2B at the extracellular level

To evaluate the potential binding complex of murine 5-HTR2B with the core of sequence of mmu-miRNA-203b-3p, we performed docking studies, combined with molecular dynamics (MD) simulations and binding energy evaluations. The average structure of murine 5-HTR2B bound to the miRNA core obtained from the last 20 ns of MD simulation is reported (Figure 4a). Briefly, the ligand forms extensive interactions with the extracellular side of the receptor, making contact with two extracellular loops (ECL2 and ECL3) and three of the seven transmembrane domains (i.e., transmembranes 5–7). Notably, the adenine of the fourth ribonucleotide (A4) of the miRNA core protrudes significantly within the receptor, thereby occupying the central portion of the extended binding pocket, which suggests that the miRNA-binding conformation is consistent with receptor activation.

Five residues, highlighted in green in Figure 4a, were primarily predicted to anchor the miRNA core to the extracellular side of the protein through a series of H-bonds. In particular, D350 from the ECL3, which forms H-bonds with the guanine moiety of G6 for almost the whole MD simulation, stabilizes the orientation of the terminal portion of the miRNA core. Meanwhile, D197 from the extracellular loop ECL2 interacted with G1 for most of the MD simulation, especially in the second half, thus fixing the binding conformation of the first three ribonucleotides. The three remaining residues, T209, K210, and K358, contribute to anchoring the central portion of the miRNA core to the extended binding pocket of the receptor. For most of the MD simulations, the positively charged side chain of K358 is positioned between the phosphate groups of A4 and G6, thus forming H-bonds with the two ribonucleotides (particularly

(**f**) 5-HT (300 μM) and CPS (1 μM) or Veh in the presence of HC-06 (30 μM), ketanserin (10 μM), or Veh and (**g**) mouse DRG neurons from *Trpv4*$^{+/+}$ and *Trpv4*$^{-/-}$ mice exposed to mmu-miR-203b-3p (10 μM), 5-HT (300 μM), CPS (10 μM), or Veh (n = 4 independent experiments). (**h**) Scratching behavior in C57BL/6J mice pretreated (0.5 hr) with ketanserin (1 mg/kg, i.p.) and induced by i.d. (10 μl) mmu-miR-203b-3p (1 nmol) or Veh. (**i**) Dose-dependent scratching behavior and wiping in C57BL/6J mice induced by 5-HT (5, 50, 500 nmol, i.d.) or Veh or (**j**) in *Trpv4*$^{+/+}$ pretreated (0.5 hr) with ketanserin (1 mg/kg, i.p.), HC-06 (10 mg/kg, i.p.), or Veh or in *Trpv4*$^{-/-}$ mice (n = 6–8 mice per group). **(j)** Typical tracings and cumulative data of the Ca^{2+} response in primary cultures of mouse skin keratinocytes exposed to mmu-miR-203b-3p (10 μM), 5-HT (300 μM), and GSK (100 nM) or Veh (n = 4 independent experiments). Dash (–) is the combination of different Vehs. Data are presented as mean ± SEM. $^{*}P < 0.05$ versus Veh and $^{§}P < 0.05$ versus GSK, rno-miR-203b-3p, 5-HT, and mmu-miR-203b-3p. Data were analyzed with one-way ANOVA with Bonferroni correction. 5-HT, serotonin; 5-HTR, serotonin receptor; Ca^{2+}, calcium ion; CI, confidence interval; CPS, capsaicin; DRG, dorsal root ganglion; EC50, half-maximal effective concentration; GSk, GSK-1016790A; HC-06, HC-067047; HEK293, human embryonic kidney 293; hr, hour; hTRPV4, human TRPV4; i.d., intradermal; i.p., intraperitoneal; KCl, potasium chloride; mDRG, mouse dorsal root ganglion; min, minute; rDRG, rat dorsal root ganglion; Veh, vehicle.

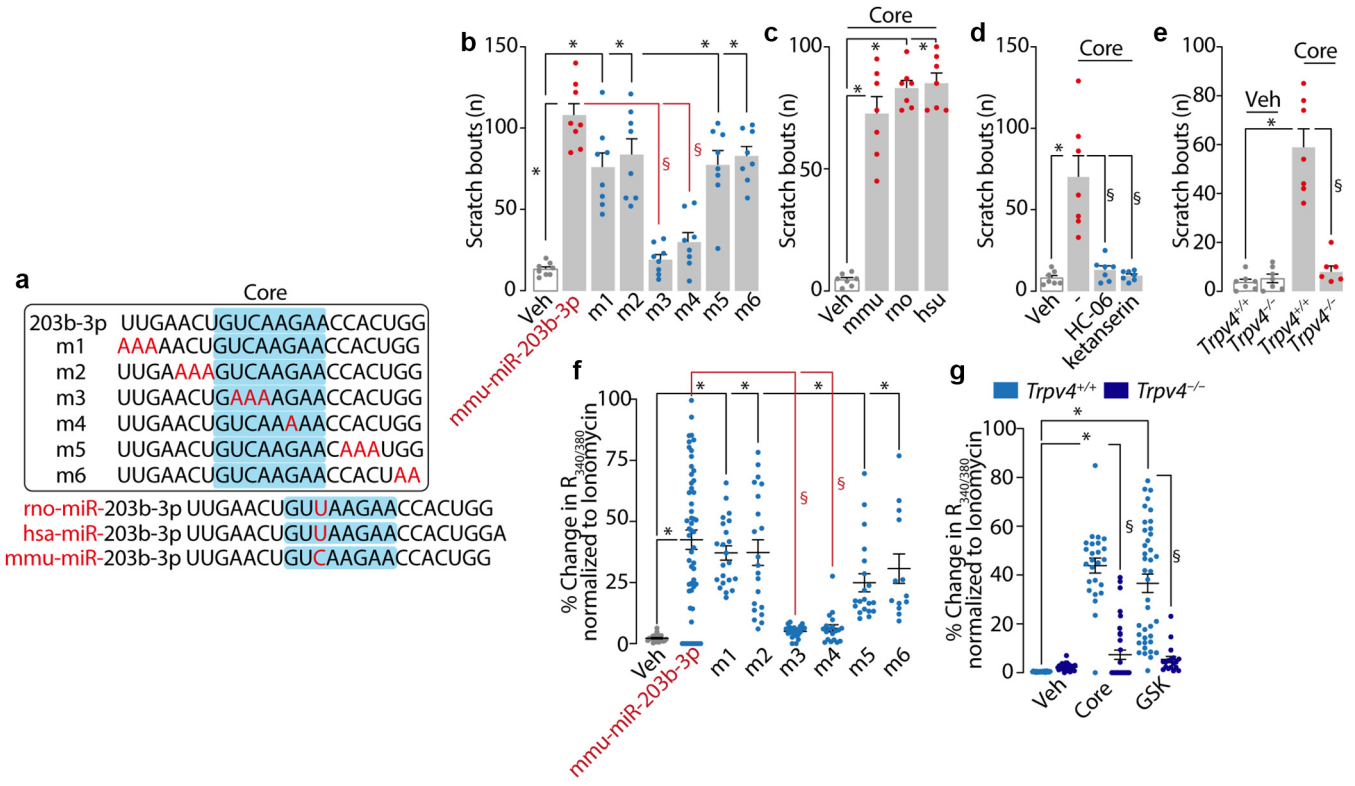

Figure 3. miRNA-203b-3p evokes scratching behavior through a conserved core sequence. (**a**) mmu-miR-203b-3p, sequence variants (m1–6), rno-miR-203b-3p, and hsa-miR-203b-3p sequences. Variated nucleotides are in red, and the core sequence of each miRNA is highlighted in light blue. (**b**) Scratching behavior in C57BL/6J mice induced by i.d. (10 μl) mmu-miR-203b-3p (1 nmol), sequence variants (m1–6, 1 nmol for all), or Veh and (**c**) core sequence of mmu-miR-203b-3p, rno-miR-203b-3p, and hsu-miR-203b-3p (1 nmol for all, i.d.) or Veh. (**d**) Scratching behavior in C57BL/6J mice induced by the core sequence of mmu-miR-203b-3p (1 nmol, i.d.) or Veh and pretreated (0.5 hr) with HC-06 (10 mg/kg, i.p.), ketanserin (1 mg/kg, i.p.), or Veh and in (**e**) *Trpv4*$^{+/+}$ and *Trpv4*$^{-/-}$ mice (n = 6–8 mice per group). (**f**) Ca^{2+} response in mouse DRG neurons exposed to mmu-miR-203b-3p (10 μM), sequence variants (m1–6, 10 μM), or Veh. (**g**) Ca^{2+} response in DRG neurons from *Trpv4*$^{+/+}$ and *Trpv4*$^{-/-}$ mice exposed to the core sequence of mmu-miR-203b-3p (10 μM), GSK (1 μM), or Veh (n = 4 independent experiments). Dash (−) is the combination of different Vehs. Data are presented as mean ± SEM. $^{*}P < 0.05$ versus Veh and $^{§}P < 0.05$ versus mmu-miR-203b-3p, core, and GSK. Data were analyzed with one-way ANOVA with Bonferroni correction. Ca^{2+}, calcium ion; DRG, dorsal root ganglion; GSK, GSK-1016790; HC-06, HC-067047; hr, hour; i.d., intradermal; i.p., intraperitoneal; miRNA, microRNA; Veh, vehicle.

with the phosphate group of G6) that help in maintaining the binding conformation of the miRNA core (Figure 4b). Similarly, T209 and K210 participate in locking the ligand to the protein extended binding pocket.

To further assess the interaction of miR-203b-3p and 5-HTR2B, primary cultures of mouse DRGs neurons were incubated with Cy3-labeled mmu-miR-203b-3p. Immunofluorescence results revealed that the Cy3-labeled mmu-miR-203b-3p but not the scrambled sequence binds to 5-HTR2B receptors on the cell surface (Figure 4c), thus confirming their interaction.

KC–sensory neuron paracrine signaling mediates the miR-203b-3p– and 5-HTR2B/TRPV4-dependent scratching behavior

To evaluate the pathophysiological implication of miR-203b-3p in psoriatic pruritus (Domingo et al., 2020; Timis and Orasan, 2018), we used a mouse model of psoriasis induced by the topical application of a cream containing imiquimod (IMQ) (5%) for 6 consecutive days, as previously described (Horváth et al., 2019; Swindell et al., 2017) (Figure 5a). Clinical signs of psoriasis measured by the PASI score (i.e., presence of erythema and scales and increase in skin thickness) were observed in IMQ-treated mice and compared with the signs in vehicle-treated (control) mice (Figure 5b and c), with no difference between male or female mice (Supplementary Figure S2a–c). Histological examination confirmed that IMQ-treated mice exhibited a time-dependent increase in epidermal thickness (Figure 5d). On day 2 after treatment, the mice developed a scratching behavior that persisted until day 7 (Figure 5e). More importantly, it was found that miR-203b-3p was overexpressed in the psoriatic back skin samples of IMQ-treated mice compared with that in the control mice (Figure 5f and g), providing evidence of the generation of pruritogenic miR-20p-03b-3p in psoriatic mouse skin samples.

Daily treatment with ketanserin or HC-06 or TRPV4 deletion attenuated the scratching behavior in IMQ-treated mice without affecting the cumulative PASI score and skin histological changes (Figure 5h–j). To confirm that miR-203b-3p eventually activates neuronal TRPV4, pSico-AAV2 containing TRPV4-targeted short hairpin RNA was injected intrathecally (lumbar 4–6) in *Adv-Cre*$^{+}$ and *Adv-Cre*$^{-}$ mice to allow for Cre-dependent *Trpv4* gene silencing specific to sensory neurons (Jung et al., 2016). Both the IMQ treatment and the subcutaneous injection of mmu-miR-203b-3p induced a scratching behavior in AAV2-*Adv-Cre*$^{-}$ mice that was attenuated in AAV2-*Adv-Cre*$^{+}$ mice (Figure 6a–c).

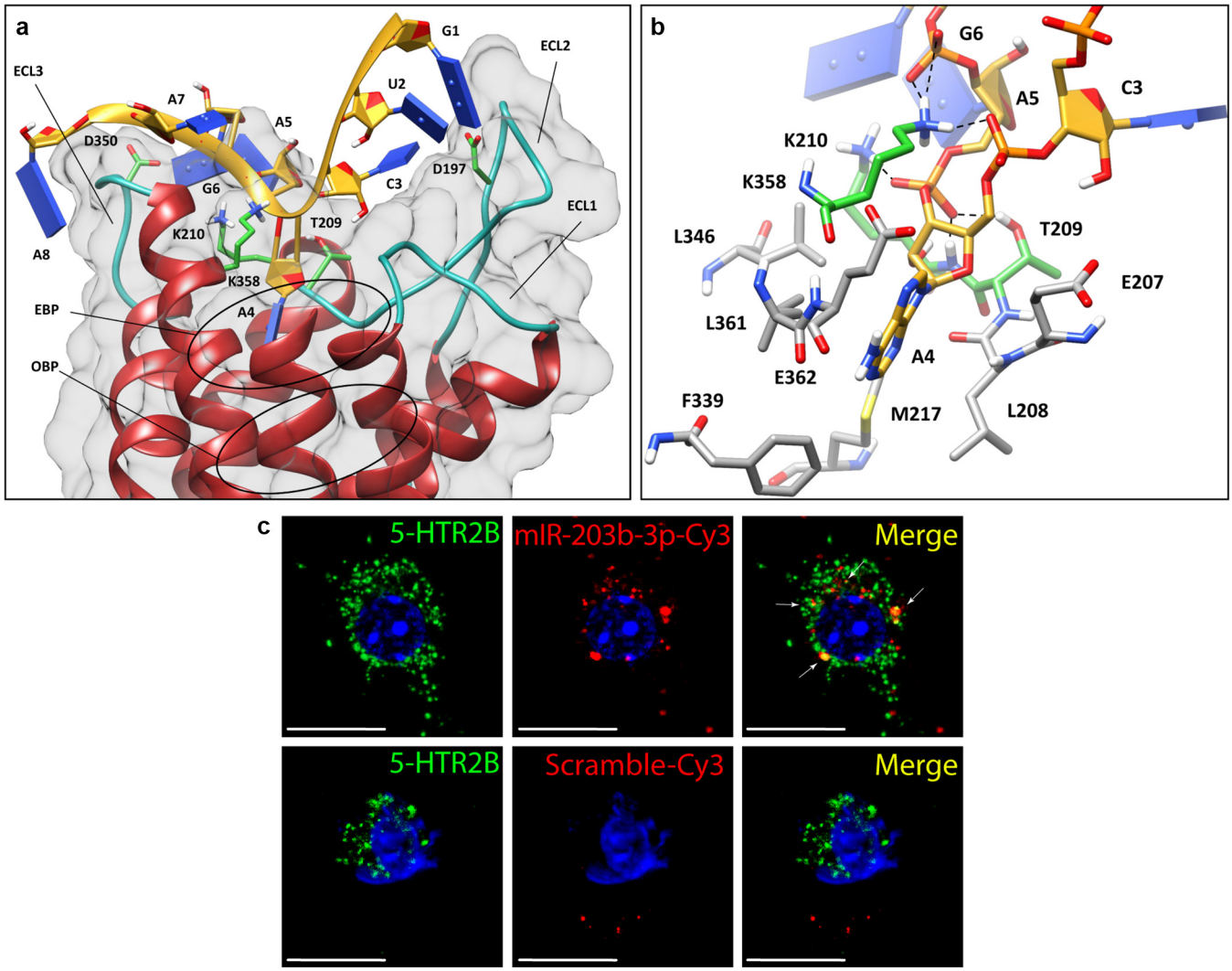

Figure 4. Computer simulation and immunofluorescence of miRNA-203b-3p binding to 5-HTR2B. (**a**) Minimized average structure of m5-HTR2B bound to the miRNA core. The phosphate backbone of the miRNA segment is shown as a gold ribbon, ribose is shown in space-filling representation, and nucleobases are displayed as blue slabs. The protein surface is shown in gray, whereas the main miRNA-anchoring residues are shown in green. The OBP and EBP are indicated together with the three ECLs (ECL1–3). (**b**) Detailed interactions formed by the central portion of the miRNA core with the EBP of m5-HTR2B. The miRNA-anchoring residues T209, K210, and K358 are shown in green, and the other proteins are shown in gray. (**c**) Live cell labeling of the binding of Cy3-labeled mmu-miR-203b-3p and Cy3-labeled scramble to 5-HTR2B on the surface of cultured mouse DRG neurons (n = 3 replicates). Bar = 20 μm. DRG, dorsal root ganglion; EBP, extended binding pocket; ECL, extracellular loop; m5-HTR2B, murine 5-HTR2B; miRNA, microRNA; OBP, orthosteric binding pocket.

It is known that the TRPV4 channel can be activated by protein kinase C (PKC)- dependent phosphorylation (Fan et al., 2009). Therefore, daily treatment with a PKC inhibitor (Ro32-0432) reduced the scratching behavior and skin histological changes evoked by IMQ but did not reduce the PASI score (Figure 6d). Moreover, the Ca^{2+} response evoked by mmu-miR-203b-3p in DRG neurons was abated by Ro32-0432 (Figure 6e). To identify the role of miR-203b-3p in the IMQ-induced scratching behavior, a complementary sequence to mmu-miR-203b-3p was tested, and the scratching behavior was reduced by daily subcutaneous injections of this complementary sequence (Figure 6f).

A considerable number of inflammatory cytokines are increased in psoriatic skin (Chen et al., 2020), including TNF-α, IL-1α, IL-6, and IL-17A (Bracke et al., 2013; Grossman et al., 1989; Mee et al., 2007; Tjabringa et al., 2008), and a multiplex array that profiles cytokines in the skin of control and IMQ-treated mice revealed that IL-1α, IL-2, IL-4, IL-6, IL-10, IL-17A, IFN-γ, TNF-α, M-CSF, G-CSF, MCP1 MIP1α, and MIP1b were increased in skin homogenates of IMQ-treated mice (Figure 6g). Using an in vitro psoriasis model (Bracke et al., 2013), we observed that exposure to a combination of TNF-α, IL-1α, IL-6, and IL-17A upregulated miR-203b-3p expression in primary cultures of mouse KCs but not in DRG neurons (Figure 6h). These findings suggest that the excitation of neuronal 5-HTR2B/TRPV4 induced by miR-203b-3p occurs through a cytokine-mediated miR-203b-3p release from KCs and not through a neuronal autocrine pathway.

Discussion

This study shows that miR-203b-3p, which is upregulated in human psoriatic skin, induced an acute scratching behavior when injected subcutaneously into mice and contributed to

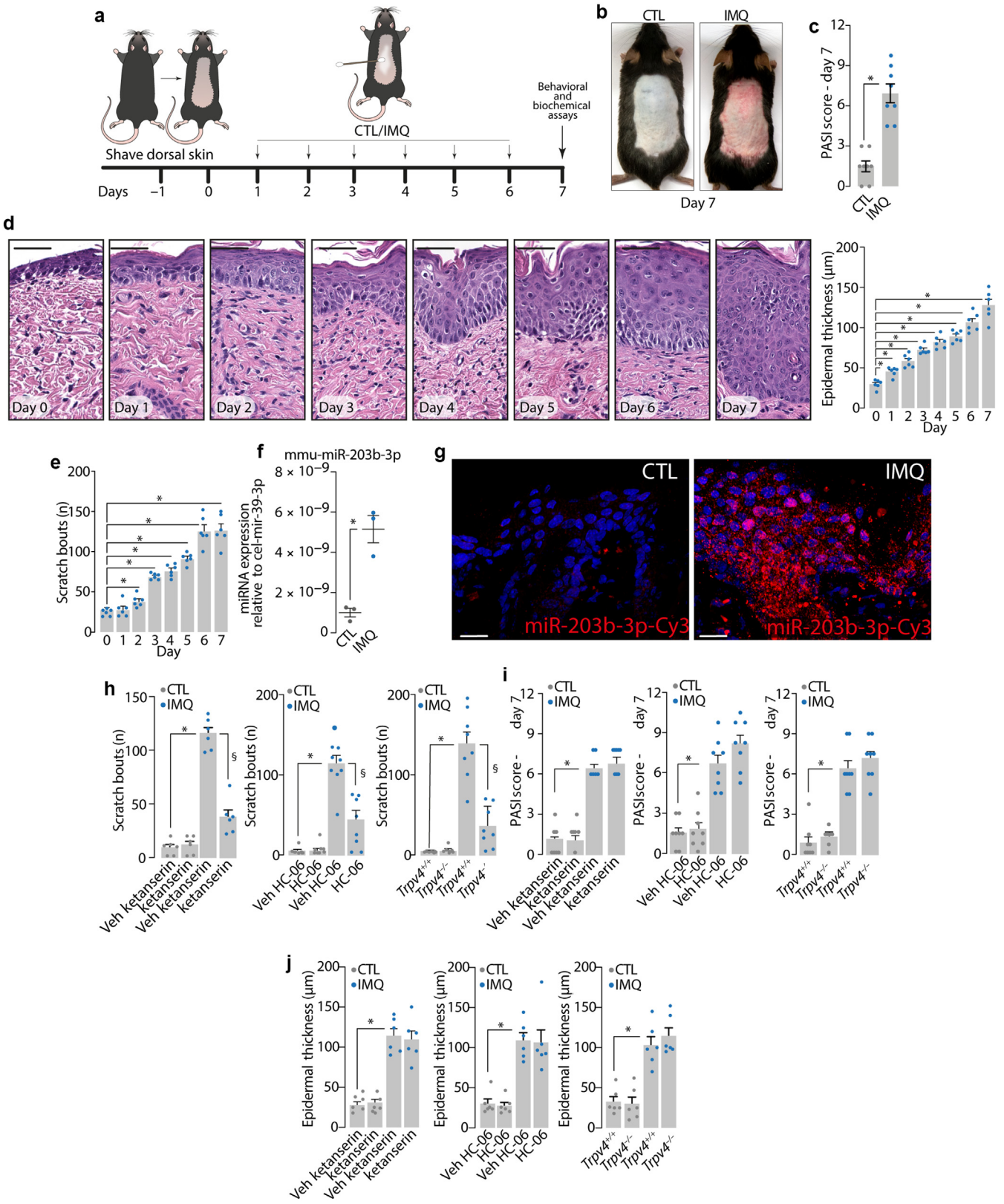

Figure 5. miR-203b-3p and 5-HTR2B/TRPV4-dependent scratching behavior in a mouse model of itch. (**a**) Treatment schedule before the behavioral test and tissue sampling in IMQ-treated or CTL (vehicle-treated) mice. (**b**) Representative photographs of the back skin of C57BL/6J mice on day 7 after IMQ or CTL treatment. (**c**) Cumulative PASI score of C57BL/6J mice on day 7 after IMQ or CTL treatment. (**d**) Representative images and cumulative data of the time-dependent (days 0–7) increase in epidermal thickness in C57BL/6J mice after IMQ treatment and (**e**) scratching behavior in C57BL/6J mice after IMQ. Bar = 20 µm. (**f**) mmu-miR-203b-3 expression relative to that of cel-mir-39-3p in psoriatic or healthy back skin samples of C57BL/6J mice on day 7 after IMQ or CTL treatment (n = 3 independent experiments). (**g**) FISH of the expression of mmu-mir-203b-3p-Cy3 in psoriatic or healthy back skin samples of C57BL/6J mice on day 7 after IMQ or CTL treatment (n = 3 replicates). Bar = 20 µm. (**h**) Scratching behavior, (**i**) cumulative PASI score, and (**j**) epidermal thickness in C57BL/6J

sustained itch in a mouse model of psoriasis. These findings extend the proposed unconventional role of miRNAs in pruritogenic signaling that was previously shown for miR-711, which produced itch in a mouse model of cutaneous T-cell lymphoma through TRPA1 (Han et al., 2018). More recent results proposed a role for miR-146a in cholestatic pruritus, where release from KCs by a TRPV4-dependent mechanism activates the neuronal TRPV1 (Chen et al., 2021). Our study provides evidence that neuronal TRPV4, which is overexpressed in chronic itching conditions (Luo et al., 2018), mediates the pruritogenic signal induced by miR-203b-3p. This is indicated by the observation that pharmacological blockade, such as total genetic deletion or selective neuronal silencing of TRPV4, protected mice from miR-203b-3p–induced scratching behavior.

Recent studies reported that TRPV4 activation induced itch through 5-HT receptors either directly (Luo et al., 2018) or indirectly (Akiyama et al., 2016; Sanjel et al., 2022). In this study, we revealed that in pruriceptive neurons, TRPV4 serves as a downstream component of the 5-HTR2B–mediated pathway needed to elicit scratching behavior by miR-203b-3p. Ca^{2+} influx recordings showed that exposure to miR-203b-3p is not sufficient per se to induce TRPV4 responses in cells transfected with either human or murine TRPV4, implying that a direct interaction between miR-203b-3p and TRPV4 is unlikely. However, the observation that Ca^{2+} responses by miR-203b-3p or 5-HT were similarly inhibited by 5-HTR2B and TRPV4 antagonism in rodent DRG neurons is consistent with the hypothesis that miR-203b-3p engages an intracellular pathway, which requires the cooperation between 5-HTR2B and TRPV4. Notably, despite the expression of a functional TRPV4, Ca^{2+} responses were absent in primary cultures of mouse KCs stimulated with miR-203b-3p, supporting the view that miR-203b-3p induces itch through direct 5-HTR2B/TRPV4 neuronal signaling without any apparent implication for non-neuronal pathways.

The GUUAAGAA core itching sequence is the portion of miR-203b-3p that targets 5-HTR2B and is conserved between different specie because the rat and human sequences were highly homologous with the murine sequence, which differ by just a single nucleotide. In addition, through a computer simulation, we predicted the potential interaction sites between miR-203b-3p and the extracellular site of 5-HTR2B consistent with receptor activation. Importantly, our three-dimensional models will facilitate future identification of ligands able to target and inactivate the function of this receptor.

Pruritus represents one of the most troublesome symptoms of psoriasis and affects the QOL of patients (Hawro et al., 2020; Remröd et al., 2015). The relief from itch is now considered to be an independent benchmark for assessing the efficacy of psoriasis treatments. Similar to other chronic itching conditions, including atopic dermatitis, itchy psoriatic skin exhibits high amounts of 5-HT (Komiya et al., 2020). Recently, a role for the TRPC4 subtype expressed by DRG neurons was reported in 5-HT–induced itch in mice with IMQ-induced psoriasis (Lee et al., 2020). A previous study showed that cutaneous mRNA expression of *TRPV4* was downregulated in the skin and was transiently upregulated in DRG neurons, along with an increase in 5-HT expression in the skin of mice in the IMQ model of psoriasis (Li et al., 2014). Although we found that genetic deletion or pharmacological antagonism of TRPV4 reduced scratching behavior in the IMQ mouse model of psoriasis, it did not ameliorate the clinical and histologic signs of psoriasis. Collectively, these findings support the hypothesis that TRPV4 is selectively involved in itch-related pathways and not in cutaneous psoriatic inflammation.

The 5-HT was found to sensitize neuronal responses to a selective TRPV4 agonist in mouse DRG neurons through PKC-dependent pathways (Cenac et al., 2010). Specifically, mice treated with a selective 5-HTR2B antagonist or a PKC inhibitor showed an attenuated scratching behavior but no reduced inflammation in response to IMQ. This suggested that 5-HTR2B, through a PKC pathway, was necessary for TRPV4-induced itch but not skin inflammation. In addition, PKC inhibition reduced Ca^{2+} responses in DRG neurons stimulated with miR-203b-3p, thus confirming the involvement of PKC in the neuronal pruritogenic pathway. Although the ability of TRPV4 to induce itch through 5-HTR2B has been previously reported (Akiyama et al., 2016; Snyder et al., 2016), in this study, we show that an intracellular pathway that implicates both receptors in DRG neurons mediates pruritus in a mouse model of a major inflammatory skin disease.

Further implications of miRNAs in psoriatic pruritus are provided by the increased expression of various proinflammatory cytokines and of miR-203b-3p in the skin of the IMQ mouse model of psoriasis. In vitro experiments showing that psoriasis-promoting cytokines increased the expression of miR-203b-3p in KCs but not in DRG neurons support the role of a paracrine pruritogenic signaling pathway. This signaling pathway involves proinflammatory cytokines that induce the release of miR-203b-3p from KCs, which targets TRPV4 activation in pruritogenic nerve terminals through 5-HTR2B. The antipruritogenic effect of a complementary sequence to mmu-miR-203b-3p in the IMQ model highlights the mechanistic relevance of this paracrine pathway in psoriatic itch.

The translational relevance of this study is two-fold. Whereas previous studies have unraveled the role of miRNAs in itch associated with malignant disease (cutaneous lymphoma) or systemic disease (cholestasis), in this study, we found that miRNAs promote itch in a mouse model of an inflammatory skin disease. This paves the way for exploring the role of miRNAs in other pruritogenic inflammatory skin diseases, including atopic dermatitis and autoimmune bullous diseases. Second, miR-203b-3p might represent a biomarker and an index of itch severity in psoriasis. Further studies could explore the skin or serum concentrations of

mice on day 7 after IMQ or CTL treatment and after the treatment (twice a day from day 1 to day 6) with ketanserin (1 mg/kg, i.p.), HC-06 (10 mg/kg, i.p.), or Veh and in *Trpv4*$^{+/+}$ and *Trpv4*$^{-/-}$ mice (n = 6–8 mice per group). Data are presented as mean ± SEM. $^{*}P < 0.05$ versus day 0 for CTL and $^{\S}P < 0.05$ versus IMQ. Data were analyzed with one-way ANOVA with Bonferroni correction. CTL, control; HC-06, HC-067047; IMQ, imiquimod; i.p., intraperitoneal; Veh, vehicle.

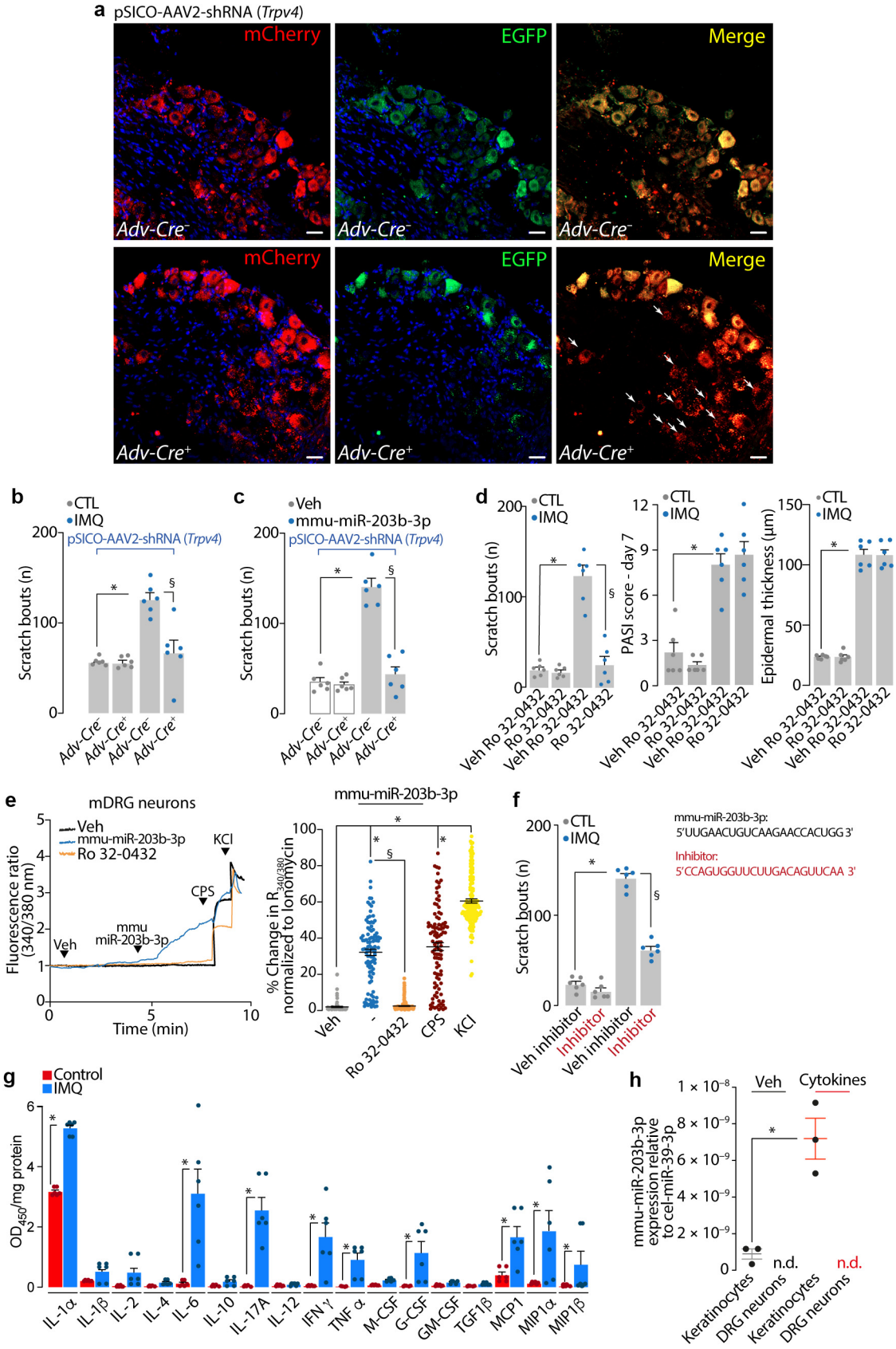

Figure 6. Selective primary sensory neurons TRPV4 silencing for the regulation of itch in the imiquimod model and inflammatory cytokines upregulating miR-203b-3p expression in mouse keratinocytes (**a**) Representative images of DRG neurons after i.th. injection with the pSico-AAV2-shRNA (*Trpv4*) viral vector in *Adv-Cre*$^{-}$ and *Adv-Cre*$^{+}$ mice. Bar = 50 µm. Scratching behavior in *Adv-Cre*$^{-}$ and *Adv-Cre*$^{+}$ mice after injection with the pSico-AAV2-shRNA (*Trpv4*) viral vector (i.th.) (**b**) on day 7 after IMQ or CTL treatment and (**c**) after i.d. (10 µl) injection of mmu-miR-203b-3p (1 nmol) or Veh. (**d**) Scratching behavior, cumulative

miR-203b-3p and their correlation with itch severity as a diagnostic and prognostic measure. Finally, our study shows that specific targeting of the itching miRNA through a complementary sequence attenuates itch in psoriatic mice, thereby highlighting miRNAs as druggable therapeutic targets. A limitation of this study is that we did not provide evidence that hsa-miRNA evokes pruritus in humans and its implication in human psoriatic itch. However, the observation that not only the murine but also the human core of miR-203b-3p elicited scratching behavior in mice points to the need for testing its ability to produce similar effects in healthy volunteers and to subsequently evaluate the beneficial effects of its complementary sequence in patients with psoriasis. The management of pruritus, which is mainly based on corticosteroids and immunosuppressants (Patel and Yosipovitch, 2010), is often unsatisfactory (Stull et al., 2016). The present and previous (Chen et al., 2021; Han et al., 2018) observations offer a therapeutic perspective for a targeted treatment of itch by disease-specific miRNAs.

MATERIALS AND METHODS

Pharmacological reagents

IMQ cream (5%) was commercially available (Aldara; 3M Pharmaceuticals, Loughborough, United Kingdom). If not otherwise indicated, reagents were obtained from Merck Life Science SRL (Milan, Italy).

Animals

Sprague-Dawley (male, 75–100 g, RRID_RGD_10395233, Charles River Laboratory, Wilmington, MA) rats were used. The following strains of mice were used: C57BL/6J mice (male and female, 25–30 g, aged 5–8 weeks, RRID_IMSR_JAX:000664, Charles River Laboratory); wild-type (*Trpa1*$^{+/+}$) and TRPA1-deficient (*Trpa1*$^{-/-}$; B6129P-Trpa1^{tm1Kykw}/J; RRID_IMSR_JAX:006401, Jackson Laboratories, Bar Harbor, ME) mice (Kwan et al., 2006), wild-type (*Trpv1*$^{+/+}$) and TRPV1-deficient (*Trpv1*$^{-/-}$; B6129X1-Trpv1^{tm1Jul}/J, RRID_IMSR_JAX:003770, Jackson Laboratories) and wild-type (*Trpv4*$^{+/+}$) and TRPV4-deficient (*Trpv4*$^{-/-}$) mice (Liedtke and Friedman, 2003), and *Advillin-Cre* (*Adv-Cre*$^{+}$ and *Adv-Cre*$^{-}$) mice (Guan et al., 2016). Genetically modified mice were all male (25–30 g, aged 5–8 weeks). The study was approved by the Italian Ministry of Health (research permits number 1194/2015-PR) and the Institutional Committee for Animal Care and Use of the Federal University of Paraná (Curitiba, Brazil) (protocols number 1234/2018).

Behavioral experiments and treatment protocol and behavioral assessment for scratching behavior

A detailed description of the method is contained in the Supplementary Materials and Methods.

Mouse model of psoriasis

Psoriasis model procedure was performed in mice as previously described (van der Fits et al., 2009). Briefly, mice were anesthetized and shaved along their backs the day before the primary IMQ cream application. IMQ cream (62.5 mg) was applied on the shaved back skin daily for 6 consecutive days. Control mice were treated similarly with a vehicle cream (vaseline).

PASI score

A detailed description of the method is contained in the Supplementary Materials and Methods.

Cell lines, primary culture of rat and mouse DRG neurons, and mouse KCs

A detailed description of the method is contained in the Supplementary Materials and Methods.

Cell transfection

The cDNA for the mouse TRPV4 was obtained by amplifying the TRPV4 plasmid GFP tagged in a high transformation efficiency strain of *Escherichia coli* (*DH5α*) with the heat and shock method (Froger and Hall, 2007) and used for transfecting HEK293 cells.

Ca^{2+} imaging

A detailed description of the method is contained in the Supplementary Materials and Methods.

Live cell labeling and immunocytochemistry in mouse DRG neurons

A detailed description of the method is contained in the Supplementary Materials and Methods.

FISH

Digoxigenin-labeled miRCURY LNA Detection probe (RRID_SCR008539) against mmu-miR-203b-3p (CAGTGGTTCTTGACAGTTCAA) and negative control (GTGTAACACGTCTATACGCCCA) were used for FISH. A detailed description of the method is contained in the Supplementary Materials and Methods.

RT-qPCR

A detailed description of the method is contained in the Supplementary Materials and Methods.

In vitro model of psoriasis

A detailed description of the method is contained in the Supplementary Materials and Methods.

Virus generation

To create the AAV plasmid for the short hairpin RNA of mouse TRPV4, a Cre-lox–conditional short hairpin RNA expression was chosen on the basis of the pSICO system (Ventura et al., 2004). A detailed description of the method is contained in the Supplementary Materials and Methods.

PASI score, and epidermal thickness in C57BL/6J mice on day 7 after IMQ or CTL treatment and after treatment with Ro32-0432 (1 mg/kg, i.p.) or Veh (n = 6 mice per group). (**e**) Typical tracings and cumulative data of the Ca^{2+} response in mouse DRG neurons exposed to mmu-miR-203b-3p (10 μM) or Veh in the presence of Ro32-0432 (100 nM) or Veh (n = 4 independent experiments) (CPS). (**f**) Scratching behavior in C57BL/6J mice on day 7 after IMQ or CTL and mmu-miR-203b-3p inhibitor (1 nmol, i.d.) or Veh (n = 6 mice per group). Data are presented as mean ± SEM. $^{*}P < 0.05$ versus CTL and $^{§}P < 0.05$ versus IMQ. Data were analyzed with one-way ANOVA with Bonferroni correction. (**g**) Cytokines/chemokines array profile in skin samples of C57BL/6J mice on day 7 after IMQ or CTL treatment (n = 6 independent experiments). (**h**) mmu-miR-203b-3p expression relative to that of cel-mir-39-3p in primary cultures of mouse keratinocytes and DRG neurons exposed to TNF-α, IL-1α, IL-6, and IL-17A (n = 3 independent experiments). Data are presented as mean ± SEM. $^{*}P < 0.05$ versus CTL and Veh and $^{§}P < 0.05$ versus IMQ. Data were analyzed with Student's *t*-test. Ca^{2+}, calcium ion; CPS, capsaicin; CTL, control; DRG, dorsal root ganglion; i.d., intradermal; IMQ, imiquimod; i.p., intraperitoneal; i.th., intrathecal; KCl, potasium chloride; n.d., not detectable; OD, optical density; shRNA, short hairpin RNA; Veh, vehicle.

miRNA measurement by RT-qPCR

RNA was purified from mouse skin samples (50 mg) and from mouse primary culture of KCs and DRG neurons treated with murine IL-1α (10 ng/ml), recombinant murine IL-6 (5 ng/ml), recombinant murine IL-17A (10 ng/ml), and recombinant murine TNF-α (5 ng/ml). Short RNAs were isolated using the miRVana miRNA isolation kit according to the manufacturer's instructions. A detailed description of the method is contained in the Supplementary Materials and Methods.

Multianalyte ELISA assay

A series of chemokines and cytokines, including IL-1α, IL-1β, IL-2, IL-4, IL-6, IL-10, IL-12, IL-17A, IFN-γ, TNF-α, M-CSF, G-CSF, GM-GSF, TGF-1β, MCP-1, MIP1α, and MIP1β, was assessed in the skin tissue from IMQ and control mice using a multianalyte ELISA array kit. A detailed description of the method is contained in the Supplementary Materials and Methods.

Molecular modeling

A detailed description of the method is contained in the Supplementary Materials and Methods.

Statistical analysis

Results are expressed as mean ± SEM. For multiple comparisons, a one-way ANOVA followed by the posthoc Bonferroni's test was used. Two groups were compared using Student's *t*-test (GraphPad Software, San Diego, CA). Half-maximal effective concentration values and confidence intervals were determined from nonlinear regression models. $P < 0.05$ was considered significant. Statistical tests used and the sample size for each analysis are listed in the figure legends.

Data availability statement

Materials and raw data generated from this study are available on request from RN (romina.nassini@unifi.it) or EA (andreeu@hotmail.com). No large datasets were generated or analyzed during this study.

ORCIDs

Francesco De Logu: http://orcid.org/0000-0001-8360-6929
Roberto Maglie: http://orcid.org/0000-0002-5106-4042
Mustafa Titiz: http://orcid.org/0000-0003-1278-6744
Giulio Poli: http://orcid.org/0000-0002-8061-5632
Lorenzo Landini: http://orcid.org/0000-0002-3933-2497
Matilde Marini: http://orcid.org/0000-0002-2199-2905
Daniel Souza Monteiro de Araujo: http://orcid.org/0000-0003-1115-725X
Gaetano De Siena: http://orcid.org/0000-0003-3600-9130
Marco Montini: http://orcid.org/0000-0001-8407-0740
Daniela Almeida Cabrini: http://orcid.org/0000-0002-7323-6933
Michel Fleith Otuki: http://orcid.org/0000-0002-0159-3878
Priscila Lúcia Pawloski: http://orcid.org/0000-0001-6231-6068
Emiliano Antiga: http://orcid.org/0000-0001-7787-4433
Tiziano Tuccinardi: http://orcid.org/0000-0002-6205-4069
João Batista Calixto: http://orcid.org/0000-0003-4041-7153
Pierangelo Geppetti: http://orcid.org/0000-0003-3797-8371
Romina Nassini: http://orcid.org/0000-0002-9223-8395
Eunice André: http://orcid.org/0000-0001-9524-1576

CONFLICT OF INTEREST

RN, FDL, and PG are founding scientists of FloNext Srl. The remaining authors state no conflict of interest.

AUTHOR CONTRIBUTIONS

Conceptualization: FDL, RM, MT, EAnt, TT, JBC, PG, RN, EAnd; Data Curation: FDL, RM, MT, EAnt, TT, JBC., PG, RN, EAnd; Formal Analysis: FDL, RM, MT, EAnt, TT, JBC., PG, RN, EAnd; Funding Acquisition: EAnd; Methodology: GP, LL, MM, DSMdA, GDS., MMo, DAC, MFO, PLP; Supervision: EA; Writing – Original Draft Preparation: FDL, RM, MT, EAnt, TT, JBC, PG, RN, EAnd, GP, LL, MM, DSMdA, GDS., MMo, DAC, MFO, PLP; Writing – Review and Editing: FDL, PG, RN, EAnd

ACKNOWLEDGMENTS

This study was supported by grants from 465430/2014-7/INCT-INOVAMED (EAnd).

SUPPLEMENTARY MATERIAL

Supplementary material is linked to the online version of the paper at www.jidonline.org, and at https://doi.org/10.1016/j.jid.2022.08.034

REFERENCES

Akiyama T, Ivanov M, Nagamine M, Davoodi A, Carstens MI, Ikoma A, et al. Involvement of TRPV4 in serotonin-evoked scratching. J Invest Dermatol 2016;136:154–60.

Bracke S, Desmet E, Guerrero-Aspizua S, Tjabringa SG, Schalkwijk J, Van Gele M, et al. Identifying targets for topical RNAi therapeutics in psoriasis: assessment of a new in vitro psoriasis model. Arch Dermatol Res 2013;305:501–12.

Caterina MJ, Pang ZX. TRP channels in skin biology and pathophysiology. Pharmaceuticals (Basel) 2016;9:77.

Cenac N, Altier C, Motta JP, d'Aldebert E, Galeano S, Zamponi GW, et al. Potentiation of TRPV4 signalling by histamine and serotonin: an important mechanism for visceral hypersensitivity. Gut 2010;59:481–8.

Chen LL, Deshpande M, Grisotto M, Smaldini P, Garcia R, He ZX, et al. Skin expression of IL-23 drives the development of psoriasis and psoriatic arthritis in mice. Sci Rep-Uk 2020;10. 1:8259.

Chen Y, Wang ZL, Yeo M, Zhang QJ, López-Romero AE, Ding HP, et al. Epithelia-sensory neuron crosstalk underlies cholestatic itch induced by lysophosphatidylcholine. Gastroenterology 2021;161:301–317. e16.

Croce CM, Calin GA. miRNAs, cancer, and stem cell division. Cell 2005;122:6–7.

De Logu F, Trevisan G, Marone IM, Coppi E, Padilha Dalenogare DP, Titiz M, et al. Oxidative stress mediates thalidomide-induced pain by targeting peripheral TRPA1 and central TRPV4. BMC Biol 2020;18:197.

Domingo S, Solé C, Moliné T, Ferrer B, Cortés-Hernández J. MicroRNAs in several cutaneous autoimmune diseases: psoriasis, cutaneous lupus erythematosus and atopic dermatitis. Cells 2020;9:2656.

Fan HC, Zhang X, McNaughton PA. Activation of the TRPV4 ion channel is enhanced by phosphorylation. J Biol Chem 2009;284:27884–91.

Froger A, Hall JE. Transformation of plasmid DNA into E. coli using the heat shock method. J Vis Exp 2007:253.

Grossman RM, Krueger J, Yourish D, Granelli-Piperno A, Murphy DP, May LT, et al. Interleukin 6 is expressed in high levels in psoriatic skin and stimulates proliferation of cultured human keratinocytes. Proc Natl Acad Sci USA 1989;86:6367–71.

Guan Z, Kuhn JA, Wang X, Colquitt B, Solorzano C, Vaman S, et al. Injured sensory neuron-derived CSF1 induces microglial proliferation and DAP12-dependent pain. Nat Neurosci 2016;19:94–101.

Han Q, Liu D, Convertino M, Wang Z, Jiang C, Kim YH, et al. miRNA-711 binds and activates TRPA1 extracellularly to evoke acute and chronic pruritus. Neuron 2018;99:449–63.e6.

Hashimoto T, Yosipovitch G. Itching as a systemic disease. J Allergy Clin Immunol 2019;144:375–80.

Hawro T, Hawro M, Zalewska-Janowska A, Weller K, Metz M, Maurer M. Pruritus and sleep disturbances in patients with psoriasis. Arch Dermatol Res 2020;312:103–11.

Hayes J, Peruzzi PP, Lawler S. MicroRNAs in cancer: biomarkers, functions and therapy. Trends Mol Med 2014;20:460–9.

Horváth S, Komlódi R, Perkecz A, Pintér E, Gyulai R, Kemény Á. Methodological refinement of Aldara-induced psoriasiform dermatitis model in mice. Sci Rep 2019;9:3685.

Jung JY, Lee SE, Hwang EM, Lee CJ. Neuronal expression and cell-type-specific gene-silencing of Best1 in thalamic reticular nucleus neurons using pSico-red system. Exp Neurobiol 2016;25:120–9.

Kittaka H, Yamanoi Y, Tominaga M. Transient receptor potential vanilloid 4 (TRPV4) channel as a target of crotamiton and its bimodal effects. Pflugers Arch 2017;469:1313–23.

Komiya E, Tominaga M, Kamata Y, Suga Y, Takamori K. Molecular and cellular mechanisms of itch in psoriasis. Int J Mol Sci 2020;21:8406.

Kwan KY, Allchorne AJ, Vollrath MA, Christensen AP, Zhang DS, Woolf CJ, et al. TRPA1 contributes to cold, mechanical, and chemical nociception but is not essential for hair-cell transduction. Neuron 2006;50:277–89.

Lee SH, Tonello R, Choi Y, Jung SJ, Berta T. Sensory neuron-expressed TRPC4 is a target for the relief of psoriasiform itch and skin inflammation in mice. J Invest Dermatol 2020;140:2221–9.e6.

Li B, Tsoi LC, Swindell WR, Gudjonsson JE, Tejasvi T, Johnston A, et al. Transcriptome analysis of psoriasis in a large case-control sample: RNA-seq provides insights into disease mechanisms. J Invest Dermatol 2014;134:1828–38.

Liedtke W, Friedman JM. Abnormal osmotic regulation in trpv4-/- mice. Proc Natl Acad Sci USA 2003;100:13698–703.

Luo JL, Feng J, Yu G, Yang P, Mack MR, Du JH, et al. Transient receptor potential vanilloid 4-expressing macrophages and keratinocytes contribute differentially to allergic and nonallergic chronic itch. J Allergy Clin Immunol 2018;141:608–19. e7.

Maglie R, Souza Monteiro de Araujo D, Antiga E, Geppetti P, Nassini R, De Logu F. The role of TRPA1 in skin physiology and pathology. Int J Mol Sci 2021;22:3065.

Mee JB, Johnson CM, Morar N, Burslem F, Groves RW. The psoriatic transcriptome closely resembles that induced by interleukin-1 in cultured keratinocytes: dominance of innate immune responses in psoriasis. Am J Pathol 2007;171:32–42.

Ohta T, Ikemi Y, Murakami M, Imagawa T, Otsuguro K, Ito S. Potentiation of transient receptor potential V1 functions by the activation of metabotropic 5-HT receptors in rat primary sensory neurons. J Physiol 2006;576:809–22.

Patel T, Yosipovitch G. Therapy of pruritus. Expert Opin Pharmacother 2010;11:1673–82.

Remröd C, Sjöström K, Svensson Å. Subjective stress reactivity in psoriasis - a cross sectional study of associated psychological traits. BMC Dermatol 2015;15:6.

Sanjel B, Kim BH, Song MH, Carstens E, Shim WS. Glucosylsphingosine evokes pruritus via activation of 5-HT2A receptor and TRPV4 in sensory neurons. Br J Pharmacol 2022;179:2193–207.

Shimada SG, LaMotte RH. Behavioral differentiation between itch and pain in mouse. Pain 2008;139:681–7.

Snyder LM, Kuzirian MS, Ross SE. An unexpected role for TRPV4 in serotonin-mediated itch. J Invest Dermatol 2016;136:7–9.

Stull C, Grossman S, Yosipovitch G. Current and emerging therapies for itch management in psoriasis. Am J Clin Dermatol 2016;17:617–24.

Sun SH, Dong XZ. Trp channels and itch. Semin Immunopathol 2016;38:293–307.

Swindell WR, Michaels KA, Sutter AJ, Diaconu D, Fritz Y, Xing XY, et al. Imiquimod has strain-dependent effects in mice and does not uniquely model human psoriasis. Genome Med 2017;9:24.

Timis TL, Orasan RI. Understanding psoriasis: role of miRNAs. Biomed Rep 2018;9:367–74.

Tjabringa G, Bergers M, van Rens D, de Boer R, Lamme E, Schalkwijk J. Development and validation of human psoriatic skin equivalents. Am J Pathol 2008;173:815–23.

Usoskin D, Furlan A, Islam S, Abdo H, Lönnerberg P, Lou D, et al. Unbiased classification of sensory neuron types by large-scale single-cell RNA sequencing. Nat Neurosci 2015;18:145–53.

van der Fits L, Mourits S, Voerman JSA, Kant M, Boon L, Laman JD, et al. Imiquimod-induced psoriasis-like skin inflammation in mice is mediated via the IL-23/IL-17 axis. J Immunol 2009;182:5836–45.

Ventura A, Meissner A, Dillon CP, McManus M, Sharp PA, Van Parijs L, et al. Cre-lox-regulated conditional RNA interference from transgenes. Proc Natl Acad Sci USA 2004;101:10380–5.

Wei JJ, Kim HS, Spencer CA, Brennan-Crispi D, Zheng Y, Johnson NM, et al. Activation of TRPA1 nociceptor promotes systemic adult mammalian skin regeneration. Sci Immunol 2020;5:eaba5683.

Wilson SR, Gerhold KA, Bifolck-Fisher A, Liu Q, Patel KN, Dong X, et al. TRPA1 is required for histamine-independent, Mas-related G protein-coupled receptor-mediated itch. Nat Neurosci 2011;14:595–602.

Wilson SR, Nelson AM, Batia L, Morita T, Estandian D, Owens DM, et al. The ion channel TRPA1 is required for chronic itch. J Neurosci 2013;33:9283–94.

Xie ZL, Hu HZ. TRP channels as drug targets to relieve itch. Pharmaceuticals (Basel) 2018;11:100.

SUPPLEMENTARY MATERIALS AND METHODS

Behavioral experiments

All behavioral experiments were in accordance with European Union guidelines for animal care procedures and the Italian legislation (DLgs 26/2014) application of the European Union Directive 2010/63/EU. The behavioral studies followed the animal research reporting in vivo experiment guidelines (Kilkenny et al., 2010). Mice were housed in a temperature- and humidity-controlled vivarium (12-hour dark/light cycle, free access to food and water, five mice per cage). At least 1 hour before behavioral experiments, mice were acclimatized to the experimental room, and behavior was evaluated between 9:00 am and 5:00 pm. All the procedures were conducted following the current guidelines for laboratory animal care and the ethical guidelines for investigations of experimental pain in conscious animals set by the International Association for the Study of Pain (Zimmermann, 1983).

The group size of n = 4–8 mice for behavioral experiments was determined by sample size estimation using G*Power (version 3.1) (Faul et al., 2007) to detect size effect in a posthoc test with types 1 and 2 error rates of 5 and 20%, respectively. Mice were allocated to vehicle or treatment groups using a randomization procedure (http://www.randomizer.org/). Investigators were blinded to the identities (genetic background) and treatments, which were revealed only after data collection. No mice were excluded from the experiments. Mice were anesthetized with a mixture of ketamine and xylazine (90 and 3 mg/kg, respectively, intraperitoneal) and killed with inhaled carbon dioxide (CO_2) plus 10–50% oxygen (O_2).

Treatment protocol

C57BL/6J (imiquimod [IMQ] or control mice) were treated with HC-067047 (10 mg/kg, intraperitoneal), ketanserin (1 mg/kg, intraperitoneal), Ro 32-0432 (1 mg/kg, intraperitoneal), or their vehicle (4% DMSO, 4% Tween 80 in 0.9% sodium chloride [NaCl]) twice a day starting from day 1 to day 6 of IMQ or vehicle treatment. C57BL/6J IMQ or control mice were treated with the complementary sequence to mmu-miR-203b-3p (1 nmol, intradermal, 10 μl, in the nape of the neck) or vehicle (0.9% NaCl) once a day starting from day 1 to day 6 of IMQ or vehicle treatment. C57BL/6J mice were injected (intradermal, 10 μl) in the nape of the neck with mmu-miR-203b-3p (0.1, 1, and 10 nmol); mmu-miR-203a-5p, mmu-miR-146-5p, mmu-miR-146-3p, mmu-miR-31-3p, mmu-miR-31-5p, mmu-miR-21-3p, and mmu-miR-21-5p (1 nmol for all) or vehicle (0.9% NaCl); mmu-miR-203b-3p sequence variants (m1–6, 1 nmol for all); mmu-miR-203b-3p, rno-miR-203b-3p, and hsa-miR-203b-3p core sequence (1 nmol for all) or vehicle (0.9% NaCl); serotonin (5-HT) (5, 50, and 500 nmol) or vehicle (0.9% NaCl); and GSK-1016790A (1, 10, 100 pmol) or vehicle (4% DMSO 4% Tween 80 in 0.9% NaCl). In a different set of experiments, C57BL/6J mice were pretreated (0.5 hours before the intradermal application of the different stimuli) with HC-067047 (10 mg/kg, intraperitoneal), ketanserin (1 mg/kg, intraperitoneal), or vehicle (4% DMSO 4% Tween 80 in 0.9% NaCl). *Trpa1*$^{+/+}$ and *Trpa1*$^{-/-}$ and *Trpv1*$^{+/+}$ and *Trpv1*$^{-/-}$ mice were injected (intradermal, 10 μl, in the nape of the neck) with mmu-miR-203b-3p (1 nmol) or vehicle (0.9% NaCl). *Trpv4*$^{+/+}$ or *Trpv4*$^{-/-}$ mice were injected (intradermal, 10 μl, in the nape of the neck) with mmu-miR-203b-3p (1 nmol), mmu-miR-203b-3p core sequence (1 nmol), or vehicle (0.9% NaCl) and 5-HT (50 nmol), GSK-1016790A (100 pmol/10 ul), or vehicle (4% DMSO 4% Tween 80 in 0.9% NaCl or 0.9% NaCl). Some *Trpv4*$^{+/+}$ mice were pretreated (0.5 hours before 5-HT) with HC-067047 (10 mg/kg, intraperitoneal), ketanserin (1 mg/kg, intraperitoneal), or vehicle (4% DMSO 4% Tween 80 in 0.9% NaCl). *Adv-Cre*$^{+}$ or *Adv-Cre*$^{-}$ mice were treated with the intrathecal (5 μl) injection of pSico-AAV2-shRNA (*Trpv4*) viral vector 4.2×10^{12} GC/ml 2 weeks before IMQ or vehicle treatment. Some C57BL/6J were injected (intradermal, 10 μl) in the cheek with mmu-miR-203b-3p (0.1, 1, and 10 nmol), 5-HT (5, 50, and 500 nmol), or vehicle (0.9% NaCl).

PASI score

The cumulative PASI score included erythema, scales, and thickening evaluation (Luo et al., 2016). Each index was scored independently on a scale from 0 to 4: 0, none; 1, slight; 2, moderate; 3, marked; and 4, maximum. The cumulative score (erythema plus scaling plus thickening) was used to measure the severity of inflammation (scale 0–12). The score for each mouse was averaged to observe changes in skin lesions.

Behavioral assessment for scratching behavior and wiping

Mice were placed into plexiglass boxes and videotaped for 60 minutes. Generally, 3–4 mice were videotaped simultaneously. Immediately after beginning videotaping, all investigators left the room. Videotapes were analyzed by investigators blinded to the treatment and genotype, and the number of scratches and wiping bouts were counted over a 60- and 30-minute period. One bout of scratching was defined as an episode in which a mouse lifted its paw and scratched continuously for any length of time until the paw was returned to the floor (Wilson et al., 2011). Hind paw movements directed away from the treated area (e.g., ear scratching) and grooming movements were not counted. A bout of wiping was defined as a continuous wiping movement with a forepaw directed at the area of the injection area (Shimada and LaMotte, 2008).

Cell lines

Human embryonic kidney 293 (HEK293) (number CRL-1573, ATCC, Manassas, VA) cells were cultured in DMEM supplemented with heat-inactivated fetal bovine serum (FBS) (10%), L-glutamine (2 mM), penicillin (100 U/ml), and streptomycin (10 mg/ml) at 37 °C in 5% CO_2 and 95% O_2. HEK293 cells stably transfected with the cDNA for the human TRPA1–HEK293 were cultured in DMEM containing heat-inactivated FBS (10%), L-glutamine (2 mM) and penicillin/streptomycin (100 U/ml), sodium pyruvate (1 mM), and G418 (1 mg/ml). HEK293 cells stably transfected with the cDNA for human TRPV1 (human TRPV1–HEK293) were grown in MEM containing heat-inactivated FBS (10%), L-glutamine (2%), and antibiotic/antimycotic solution (2%) and selected with G418 (1 μl/ml). HEK293 cells stably transfected with the cDNA for human TRPV4 (human TRPV4–HEK293) were cultured in DMEM containing FBS tetracycline free (10%), hygromycin B

(100 μg/ml), and blasticidin S hydrochloride (5 μg/ml). Tetracycline (0.1 μg/ml) was added overnight before calcium imaging experiments. All cells were used when received without further authentication.

Primary culture of rat and mouse dorsal root ganglion neurons

Dorsal root ganglions (DRGs) (combined cervical, thoracic, and lumbar) were bilaterally excised under a dissection microscope and enzymatically digested using 2 mg/ml of collagenase type 1A and 1 mg/ml of trypsin for rat DRG neurons or 2 mg/ml of collagenase type 1A and 1 mg/ml of papain for mouse DRG neurons in Hanks' Balanced Salt Solution for 35 minutes at 37 °C. Ganglia were disrupted by several passages through a series of syringe needles (23–25 G). Rat and mouse neurons were then pelleted by centrifugation at 1,200 r.p.m. for 5 minutes at room temperature (RT) and resuspended in DMEM supplemented with 10% heat-inactivated horse serum (rat DRG neurons) or Ham's-F12 (mouse DRG neurons), both containing 10% heat-inactivated FBS, 100 U/ml of penicillin, 0.1 mg/ml streptomycin, and 2 mM L-glutamine added with 100 ng/ml nerve GF and 2.5 mM cytosine-b-D-arabino-furanoside free base and maintained at 37 °C in 5% CO_2 and 95% O_2 for 3 days before being used for calcium imaging experiments.

Primary culture of mouse tail keratinocytes

The mouse tail was cut off, and the skin was peeled off and cut into smaller pieces (2–3 cm). The peeled skin was digested in 4 mg/ml dispase in keratinocytes (KCs) growth medium (EpiVita, Cell Applications, San Diego, CA) at 4 °C overnight. The day after, tissue was washed in PBS to remove excessed dispase, and the dermis was slowly lifted up and away from the epidermis. The separated epidermis was put and floated on drops (500 μl) of trypsin-EDTA solution (0.25%), with the basal layer downward the skin on a petri dish at RT on a horizontal shaker with gentle agitation. After 20 minutes, KCs growth medium was added to the petri dish, and the epidermis was grasped using forceps and vigorously rubbed back and forth to release single cells from the epidermal sheet. These passages were repeated three times. The cell clumps were broken using a serological pipette and then passed the cell solution through a 100-μm filter. The filtered cells were centrifuged for 5 minutes at 180*g* and seeded in culture dishes precoated with bovine collagen I (5 μg/ml) and put at 37 °C in 5% CO_2 and 95% O_2 until reaching confluence. KC terminal differentiation was induced by adding calcium chloride (0.2 mM) to the culture medium (Li et al., 2017).

Primary culture of mouse epidermal KCs

The dorsal skin (approximately 9 cm^2) of four mice was removed and placed hairy-side down in a petri dish, and all subcutaneous tissues were scraped under sterile condition. The skin was sliced into 0.5 × 1–1.5 cm strips using a scalpel and placed hairy-side up on the surface of 20 ml of PBS added with trypsin (0.25%) for 2 hours at 32 °C. Floating skin strips were transferred to a new petri dish containing KCs growth medium, and the epidermis was scraped off using a scalpel blade and forceps. The medium containing scraped epidermal cells and the skin strips was collected into a sterile 60 ml jar with a magnetic stir bar and stirred at 100 r.p.m. for 20 minutes at RT. The content was passed through a 70-μm cell strainer filter. The cell filtrate was centrifuged at 160*g* for 7 minutes at 4 °C, the pellet was resuspended by gently triturating with a 5-ml pipet, and cells were plated on 35-mm glass coverslips precoated with bovine collagen I (5 μg/ml) and maintained at 32 °C in 5% CO_2 and 95% O_2 for 24 hours (Morris et al., 2019).

Cell transfection

After reaching 50–70% confluence in a 24 multiwell plate, cells were incubated with 8.4 μg/ml of plasmid DNA in OptiMEM in the presence of transfection reagent TransIT (MIRUS Optimization protocol for plasmid DNA delivery) for 72 hours. Transfected cells were grown in MEM containing 10% heat-inactivated FBS, 100 U/ml of penicillin, and 0.1 mg/ml of streptomycin plus neomycin 250 μg/ml.

Calcium imaging

Cells were plated on poly-L-lysine–coated (8.3 μM) 35-mm glass coverslips (Thermo Fisher Scientific, Waltham, MA) and maintained at 37 °C in 5% CO_2 and 95% O_2 for 24 hours. Cells were loaded (40 minutes) with Fura-2 AM-ester (5 μM) added to the buffer solution (37 °C) containing (in mM) 2 calcium chloride, 5.4 potassium chloride, 0.4 magnesium sulfate, 135 NaCl, 10 D-glucose, 10 4-(2-hydroxyethyl)-1-piperazineethanesulfonic acid, and BSA (0.1%) at pH 7.4. Cells were washed and transferred to a chamber on the stage of a fluorescent microscope for recording (Olympus IX 81, Olympus, Tokyo, Japan). Human TRPA1–HEK293, human TRPV1–HEK293, human TRPV4–HEK293, mouse TRPV4–HEK293 cells, and rat and mouse DRG neurons were exposed to has-, mmu-, and rno-miR-203b-3p (10 nM–100 μM), serotonin (10 nM–3 mM), mmu-miR-203b-3p sequence variants (m1–6, 10 μM for all), allyl isothiocyanate (10 μM), capsaicin (1–10 μM), GSK-1016790A (10 nM–10 μM), and potassium chloride (50 mM). The calcium ion response was monitored in the presence of ketanserin (10 μM), HC-067047 (30 μM), capsazepine (30 μM), or vehicle (0.1–0.3 % DMSO) and Ro32-0432 (100 nM) or its vehicle (0.001% DMSO) in mouse DRG neurons. A high concentration (50 mM) of potassium chloride that depolarizes functional neurons causing calcium ion influx was used to further exclude the non-neuronal cells. Mouse epidermal KCs were exposed to mmu-miR-203b-3p (10 μM), GSK-1016790A (100 nM), serotonin (300 μM), or vehicle (0.001% DMSO). Results were expressed as the percent increase in ratio 340/380 over baseline normalized to the maximum effect induced by ionomycin (5 μM) added at the end of each experiment.

Live cell labeling and immunocytochemistry in mouse DRG neurons

DRG neurons were plated on poly-L-lysine (8.3 μM)- and laminin (5 μM)-coated 35-mm glass coverslips (Thermo Fisher Scientific) and maintained at 37 °C in 5% CO_2 and 95% O_2 for 24 hours. Cells were incubated with Cy3-labeled miR-203b-3p or Cy3-scramble-miR-203b-3p-m2 (RRID_SCR_001363), 1 mM diluted in extracellular cell solution, for 15 minutes at 37 °C in 5% CO_2 and 95% O_2. Coverslips were washed and incubated with 5-HTR2B

primary antibody (1:1,000, RRID_SCR012931) at RT for 1 hour. The cells were incubated with the fluorescent polyclonal secondary antibody Alexa Fluor 488 (1:600; RRID_SCR008410) and examined with a Zeiss AxioImager2 microscope in a z-stack and Apotome mode (Carl Zeiss Spa, Milan, Italy).

FISH

Anesthetized mice were transcardially perfused with PBS and 4% paraformaldehyde, and the skin was dissected and fixed overnight with 4% paraformaldehyde. Frozen sections (14 μm) were washed in PBS added with 0.1% Tween 20 and acetylated for 10 minutes with triethanolamine and acetic anhydride to prevent nonspecific binding of the probe. Sections were then incubated with proteinase K (1:20,000; stock solution 20 μg/μl; RRID_SCR 001326) for 10 minutes, followed by a fixation with 4% paraformaldehyde for 15 minutes at RT. The tissue was prehybridized in a hybridization buffer at 60 °C for 1 hour, and the probes were diluted with a hybridization buffer to 50 nM and hybridized at 60 °C overnight. Sections were then washed with PBS added with 0.1% Tween 20 and blocking solution (RRID_SCR 001326) diluted in maleic acid buffer with Tween 20 for 30 minutes at RT and then incubated with alkaline phosphatase–conjugated anti-DIG (1:2,000; RRID_SCR 001326) at 4 °C overnight. After washing with PBS added with 0.1% Tween 20 and alkaline phosphatase inhibition buffer (0.1 M NaCl, 0.1 M Tris-hydrogen chloride, pH 9.5, 0.05 M magnesium chloride, 0.1% Tween 20), the in situ signals were developed with a fast red substrate (RRID_SCR 001326) (1 tablet in 2 ml 0.1 M Tris-hydrogen chloride, pH 8.2) for 3 hours. Slides were then washed in PBS added with 0.1% Tween 20 and coverslipped using a mounting medium with DAPI (RRID_SCR012931). The images were captured by a Zeiss AxioImager2 microscope in a z-stack and Apotome mode (Carl Zeiss Spa).

qRT-PCR

Total RNA was extracted from mouse and rat DRGs. The standard TRIzol extraction method was used together with RNeasy Mini Kit (RRID_SCR008539) according to the manufacturer's instructions. RNA concentration and purity were assessed spectrophotometrically by measuring the absorbance at 260–280 nm. The RNA purified from DRGs was reverse transcribed using SuperScript IV VILO master mix with ezDNase enzyme according to the manufacturer's instructions. The KAPA SYBR FAST universal kit was used for the amplification, and the cycling conditions were as follows: samples were heated to 95 °C for 10 minutes followed by 40 cycles of 95 °C for 10 seconds and 65 °C for 20 seconds. PCR reaction was performed in triplicate for each sample. Relative expression of mRNA was calculated using the $2^{-\Delta(\Delta CT)}$ comparative method, with each gene normalized against the *β-actin*. For relative quantification of mRNA compared with that of housekeeping gene, real-time PCR was carried out using Rotor Gene Q (Qiagen, Hilden, Germany). The sets of primers for mice and rats are listed in Supplementary Table S1.

Virus generation

The construct AAV2-EF1-mCherry-SICO-GFP-mTRPV4-shRNA was purchased from Vector BioLabs (Malvern, PA). The conditional expression of mouse TRPV4 short hairpin RNA (shRNA) (5′ CACCGCAACATGCGTGAATTCATCACT CGAGTGATGAATTCACGCATGTTGC TTTTTT-3′; ref sequence number NM_022017) is regulated through the recognition of two modified loxP sites (named TATAlox) by Cre, which recombines the pSICO vector exciding the CMV-eGFP cassette and flanking the TATAlox-shRNA sequence next to the U6 promoter. The recombination replaces the correct spacing between the promoter and the transcription start site, resulting in the transcription of mouse TRPV4 shRNA. In the absence of Cre, the CMV-eGFP cassette is placed between the U6 promoter and the shRNA transcription start site, avoiding the expression of mouse TRPV4 shRNA. Otherwise, mCherry expression is constitutive under an EF1 promoter. AAV2 was used at a viral titer of 4.2×10^{12} GC/ml (Vector BioLabs).

In vitro model of psoriasis

For in vitro model mimicking the psoriasis phenotype, mouse primary culture of KCs and DRG neurons was plated in six-well plates (Thermo Fisher Scientific) and maintained in 5% CO_2 and 95% O_2 (24 hours, 37 °C). The medium was added with recombinant murine IL-1α (10 ng/ml), recombinant murine IL-6 (5 ng/ml), recombinant murine IL-17A (10 ng/ml), and recombinant murine TNF-α (5 ng/ml), and cells were maintained in 5% CO_2 and 95% O_2 overnight at 37 °C before the extraction and measurement of microRNA (miRNA) by qRT-PCR.

miRNA measurement by qRT-PCR

Briefly, total RNA samples were mixed with five volumes of lysis/binding buffer and 1/10 volume of miRNA homogenate additive and left on ice for 10 minutes. A low concentration of ethanol (25% v/v) was then added to the samples, which were subsequently mixed and bound to a filter cartridge by centrifugation. The relatively low concentration of ethanol in this first treatment allows the binding of the larger RNAs to the column, whereas the shorter, more soluble RNAs pass through and are collected. In the second step, a higher concentration of ethanol was added to the eluant (40% v/v), allowing the shorter RNAs to be immobilized to filter cartridges during centrifugation and subsequently eluted. All RNA samples were immediately used or kept at −80 °C until further processing. Reverse transcription reactions were performed using the TaqMan Advanced miRNA cDNA Synthesis Kit, following the manufacturer's instructions. For mRNA relative quantification, qPCR was performed on Rotor Gene Q (Qiagen) using TaqMan Fast Advanced Master Mix (2×) and TaqMan Advanced miRNA Assay specific for mmu-miR-203b-3p (stem-loop accession number MI0040622) and for cel-miR-39-3p (stem-loop accession number MI0000010). Relative quantities of miRNAs were calculated using the $2^{-\Delta(\Delta CT)}$ comparative method after normalization to the spiked-in control *Caenorhabditis elegans* miRNA-39 (cel-miRNA-39).

Multianalyte ELISA assay

Briefly, skin samples were dissected from killed IMQ and control mice, homogenized in PBS (0.1 M) with a tissue homogenizer (Qiagen) for 30 seconds, and centrifuged at 10,000*g* for 10 minutes, and the supernatants were collected and assayed according to the manufacturer's instructions. Samples were assayed in triplicate. The raw data obtained from the absorbance (optical density 450 nm) readings were normalized to the milligram of protein.

Molecular modeling

Because no X-ray structure of murine 5-HTR2B (m5-HTR2B) is currently available, a three-dimensional model of the protein was generated on the basis of the X-ray structure of human 5-HTR2B (h5-HTR2B) in complex with the agonist ligand ergotamine (Protein Data Bank-PDB code 4IB4) (Wacker et al., 2013). The core sequence of the miRNA was docked on the extracellular side of the m5-HTR2B model using Gold software, generating 100 different potential binding modes. The 22 most reliable binding modes selected after a careful visual inspection and postdocking filtering were further analyzed through molecular dynamics (MD) simulation studies. The corresponding miRNA–protein complexes were embedded in a lipid bilayer; solvated with explicit water molecules; and subjected to an MD protocol, including a three-step energy minimization, brief heating and equilibration stages, and a final production stage of 25–50 ns of MD simulation. The seven most stable complexes in terms of root-mean-square deviation (RMSD) of the miRNA core during the MD were then analyzed from an energetic point of view by performing miRNA–protein binding free energy evaluations using the Molecular Mechanics Poisson–Boltzmann Surface Area approach. The obtained results strongly suggested complex 11 as the most energetically favored one because the binding energy associated with this complex (−78.5 kcal/mol) was significantly better than those associated with the other complexes (Supplementary Table S2). On the basis of the whole computational analysis, complex 11, which also showed the lowest miRNA RMSD value during the whole 50 ns of MD simulation (average RMSD = 4.4 Å) (Supplementary Table S3), was considered the most reliable miRNA–protein complex.

Protein structure refinement and modeling. Molecular modeling studies were performed using a model of m5-HTR2B receptor generated on the basis of the X-ray structure of the h5-HTR2B because the two isoforms presented >80% sequence identity. Considering the hydrophilic nature of miRNAs and the presence of a well-known ligand-binding site located on the extracellular side of 5-HTR2B, which can accommodate various small-molecule ligands endowed with agonist activity, we envisioned that the miRNA core could interact with m5-HTR2B on its extracellular side, occupying at least part of the ligand-binding pocket. On the basis of these considerations, the X-ray structure of h5-HTR2B in complex with ergotamine (PDB code 4IB4) (McCorvy et al., 2018) was selected as a reference. In fact, ergotamine interacts with a wide portion of the extracellular side of the receptor, encompassing both the supposed orthosteric binding pocket, buried within the transmembrane protein region and occupied by the ergoline core of the ligand and a shallower region occupied by the benzyltripeptide moiety of the agonist that can be referred to as extended binding pocket (EBP). To obtain an optimal template for modeling the structure of the m5-HTR2B, the reference protein structure was initially refined by replacing residues 195–206 of the partially unresolved extracellular loop ECL2 with the corresponding residues belonging to the X-ray structure of h5-HTR2B in complex with methysergide (PDB code 6DRZ), in which the loop was fully solved (McCorvy et al., 2018). All protein residues that did not belong to h5-HTR2B were removed, whereas the missing side chains of partially unresolved h5- HTR2B residues were automatically reconstructed using Modeller software (Webb and Sali, 2007). The refined structure was eventually subjected to energy minimization in an explicit water environment after being embedded in a lipid bilayer. The generation of the phospholipid bilayer composed of POPC (1-palmitoyl-2-oleoyl-sn-glycero-3-phosphocholine) molecules and the insertion of the receptor within it were performed using Visual Molecular Dynamics software (Humphrey et al., 1996). The energy minimization was then carried out with AMBER software, version 16 (Case et al., 2016). The system was solvated with a 15 Å water cap on both the intracellular and the extracellular sides using the TIP3P solvent model, whereas sodium ions were added as counterions to neutralize the system. The Lipid14 parameters were assigned to POPC molecules. Three sequential minimization stages, each consisting of 5,000 steps of steepest descent followed by conjugate gradient, were thus performed. In the first stage, a position restraint of 100 kcal/mol·Å^2 was applied to the whole protein and phospholipid bilayer to uniquely minimize the positions of the water molecules. In the second stage, the same position restraint was only applied to the protein residues, thus leaving the phospholipid molecules free, whereas in the last stage, only the protein α-carbons were restrained with a harmonic potential of 30 kcal/mol·Å^2. The refined h5-HTR2B structure was then used as a template for modeling the structure of m5-HTR2B using Modeller software. A total of 100 different models of m5-HTR2B were generated on the basis of the refined h5-HT2BR structure, and the model presenting the best value of discrete optimized protein energy score was then selected and subjected to the same energy minimization protocol applied to the template structure. The energy minimized structure was thus considered as the final m5-HTR2B model, which was used for docking and MD simulation studies.

Protein–RNA docking studies. The three-dimensional structure of the murine miRNA-203b-3p core was automatically built, directly from its sequence, using the modeling webserver RNAComposer (Popenda et al., 2012). The generated miRNA core was then docked into the energy-minimized model of m5-HT2BR using gold software with Piecewise Linear Potential (PLP) fitness function (Verdonk et al., 2003). Considering the dimensions of the miRNA core sequence, to take into account a proper portion of the receptor for the docking calculations, including both the supposed orthosteric binding pocket and the EBP, the docking site was manually defined on the basis of a selected series of residues. The residues defining the binding site included the

homolog residues of h5-HTR2B located in a range of 10 Å from the tripeptide portion of ergotamine in the reference complex (PDB code 4IB4) and the remaining extracellular portions of the receptor. A total of 100 different docking solutions were generated by the docking procedure. The predicted binding orientations of the miRNA core were then visually inspected and filtered according to different criteria. Initially, unreliable binding modes in which the miRNA core protruded into regions that should be occupied by the phospholipid membrane surrounding the protein were discarded. Similarly, docking solutions in which the disposition of the miRNA core was not consistent with the presence of the additional ribonucleotides of the full miRNA sequence were discarded as well. The retained binding modes were then further analyzed to select those in which the miRNA core sufficiently occupied the binding site of the receptor. For this purpose, we selected all docking solutions in which the miRNA core presented at least one atom in the range of 5 Å from L361. This residue, located in EBP, is the conserved homolog residue of L362 in h5-HT2BR, which was found to be an interaction site essential for the agonist effect of lysergic acid diethylamide and responsible for an auxiliary mechanism of agonist activation of h5-HTR2B through the EBP (McCorvy et al., 2018). For this reason, the proximity of the miRNA core to this residue was used as a criterion for selecting reliable binding modes consistent with receptor activation, in which the miRNA core sufficiently occupied at least the EBP of the receptor. Using these filters, 22 reliable binding dispositions were eventually selected and considered for further analyses.

MD simulations. All MD simulations were carried out with AMBER 16. The 22 RNA–protein complexes generated by docking were inserted in a lipid bilayer of POPC molecules and solvated with a 15 Å water cap on both the intracellular and extracellular sides, as performed for the energy minimization described earlier. TIP3P was used as the solvent model, including sodium ions to neutralize the systems. For each complex, the three sequential minimization steps described earlier were initially performed. Subsequently, as performed in previous MD protocols applied for studying transmembrane receptors (Bizzarri et al., 2019; De Logu et al., 2019), the temperature of the system was gradually raised from 0 to 300 K through a brief constant-volume MD simulation where a position restraint of 30 kcal/mol·Å^2 was applied on the protein α-carbons. The system was then relaxed through a 500 ps constant-pressure MD simulation in which the harmonic potential applied to the protein α-carbons was decreased to 10 kcal/mol·Å^2, and Langevin thermostat was used to maintain the temperature at 300 K. Finally, 25 ns of constant-pressure MD simulation production were performed using the Monte Carlo barostat with anisotropic pressure scaling. In this MD stage, the position restraints on the protein extracellular loops were removed, so that they could fully adapt their conformation to the bound miRNA core. For each complex, the stability of the miRNA core–binding conformation during the production stage of the MD simulation was analyzed in terms of RMSD of the miRNA phosphorous atoms. The results showed that in a few cases, the miRNA core partially detached from the protein, completely losing the initial binding mode predicted by docking, as highlighted by an average RMSD value >10 Å (Supplementary Table S4). An additional MD production stage of 25 ns was then performed for the 11 complexes in which the average RMSD of the miRNA phosphorous atoms during the MD, with respect to their initial disposition, did not exceed the value of 6.0 Å. The other complexes were instead discarded. The RMSD analysis was then repeated for the 11 complexes considering the full simulation time of 50 ns: in this case, only four complexes (with average miRNA RMSD > 6.0 Å) were discarded (Supplementary Table S3), and the remaining seven complexes were selected for binding energy evaluations. All simulations were performed using particle mesh Ewald electrostatics with a cutoff of 10 Å for nonbonded interactions and periodic boundary conditions. A simulation step of 2.0 fs was employed because all bonds involving hydrogen atoms were kept rigid using the SHAKE algorithm. The Lipid14 parameters were assigned to POPC molecules, whereas RNA.OL3 parameters were used for the miRNA core.

Binding energy evaluations. The evaluation of the binding energy associated with the seven most reliable miRNA–protein complexes analyzed through MD simulations was carried out using AMBER 16, as previously described (Poli et al., 2018; Tuccinardi et al., 2007). The trajectories relative to the last 20 ns of each simulation were extracted and used for the calculation, for a total of 200 snapshots (at time intervals of 100 ps). Van der Waals electrostatic and internal interactions were calculated with the SANDER module of AMBER 16, whereas polar energies were calculated using the Poisson–Boltzmann methods with the Molecular Mechanics Poisson–Boltzmann Surface Area module of AMBER 16. Dielectric constants of 1 and 80 were used to represent the gas and water phases, respectively, whereas the MOLSURF program was employed to estimate the nonpolar energies.

SUPPLEMENTARY REFERENCES

Bizzarri BM, Botta L, Aversa D, Mercuri NB, Poli G, Barbieri A, et al. L-dopaquinone mediated recovery from GIRK channel firing inhibition in dopaminergic neurons. ACS Med Chem Lett 2019;10:431–6.

Case DA, Betz RM, Cerutti DS, Cheatham TEI, Darden TA, Duke RE, et al. AMBER 2016. San Francisco, CA. San Francisco: University of California; 2016.

De Logu F, Li Puma S, Landini L, Tuccinardi T, Poli G, Preti D, et al. The acyl-glucuronide metabolite of ibuprofen has analgesic and anti-inflammatory effects via the TRPA1 channel. Pharmacol Res 2019;142:127–39.

Faul F, Erdfelder E, Lang AG, Buchner AG. *Power 3: a flexible statistical power analysis program for the social, behavioral, and biomedical sciences. Behav Res Methods 2007;39:175–91.

Humphrey W, Dalke A, Schulten K. VMD: visual molecular dynamics. J Mol Graph 1996;14. :33–8, 27–8.

Kilkenny C, Browne WJ, Cuthill IC, Emerson M, Altman DG. Improving bioscience research reporting: the ARRIVE guidelines for reporting animal research. PLoS Biol 2010;8:e1000412.

Li F, Adase CA, Zhang LJ. Isolation and culture of primary mouse keratinocytes from neonatal and adult mouse skin. J Vis Exp 2017;125:56027.

Luo DQ, Wu HH, Zhao YK, Liu JH, Wang F. Original Research: different imiquimod creams resulting in differential effects for imiquimod-induced psoriatic mouse models. Exp Biol Med (Maywood) 2016;241:1733–8.

McCorvy JD, Wacker D, Wang S, Agegnehu B, Liu J, Lansu K, et al. Structural determinants of 5-HT2B receptor activation and biased agonism. Nat Struct Mol Biol 2018;25:787–96.

Morris RJ, Readio N, Boland K, Johnson K, Lad S, Singh A, et al. Isolation of mouse epidermal keratinocytes and their in vitro clonogenic culture. J Vis Exp 2019;150.

Poli G, Lapillo M, Granchi C, Caciolla J, Mouawad N, Caligiuri I, et al. Binding investigation and preliminary optimisation of the 3-amino-1,2,4-triazin-5(2H)-one core for the development of new Fyn inhibitors. J Enzyme Inhib Med Chem 2018;33:956–61.

Popenda M, Szachniuk M, Antczak M, Purzycka KJ, Lukasiak P, Bartol N, et al. Automated 3D structure composition for large RNAs. Nucleic Acids Res 2012;40:e112.

Shimada SG, LaMotte RH. Behavioral differentiation between itch and pain in mouse. Pain 2008;139:681–7.

Tuccinardi T, Manetti F, Schenone S, Martinelli A, Botta M. Construction and validation of a RET TK catalytic domain by homology modeling. J Chem Inf Model 2007;47:644–55.

Verdonk ML, Cole JC, Hartshorn MJ, Murray CW, Taylor RD. Improved protein-ligand docking using gold. Proteins 2003;52:609–23.

Wacker D, Wang C, Katritch V, Han GW, Huang XP, Vardy E, et al. Structural features for functional selectivity at serotonin receptors. Science 2013;340:615–9.

Webb B, Sali A. Comparative protein structure modeling using MODELLER. Curr Protoc Protein Sci 2007. Chapter 2:Unit 2.9.

Wilson SR, Gerhold KA, Bifolck-Fisher A, Liu Q, Patel KN, Dong X, et al. TRPA1 is required for histamine-independent, Mas-related G protein-coupled receptor-mediated itch. Nat Neurosci 2011;14:595–602.

Zimmermann M. Ethical guidelines for investigations of experimental pain in conscious animals. Pain 1983;16:109–10.

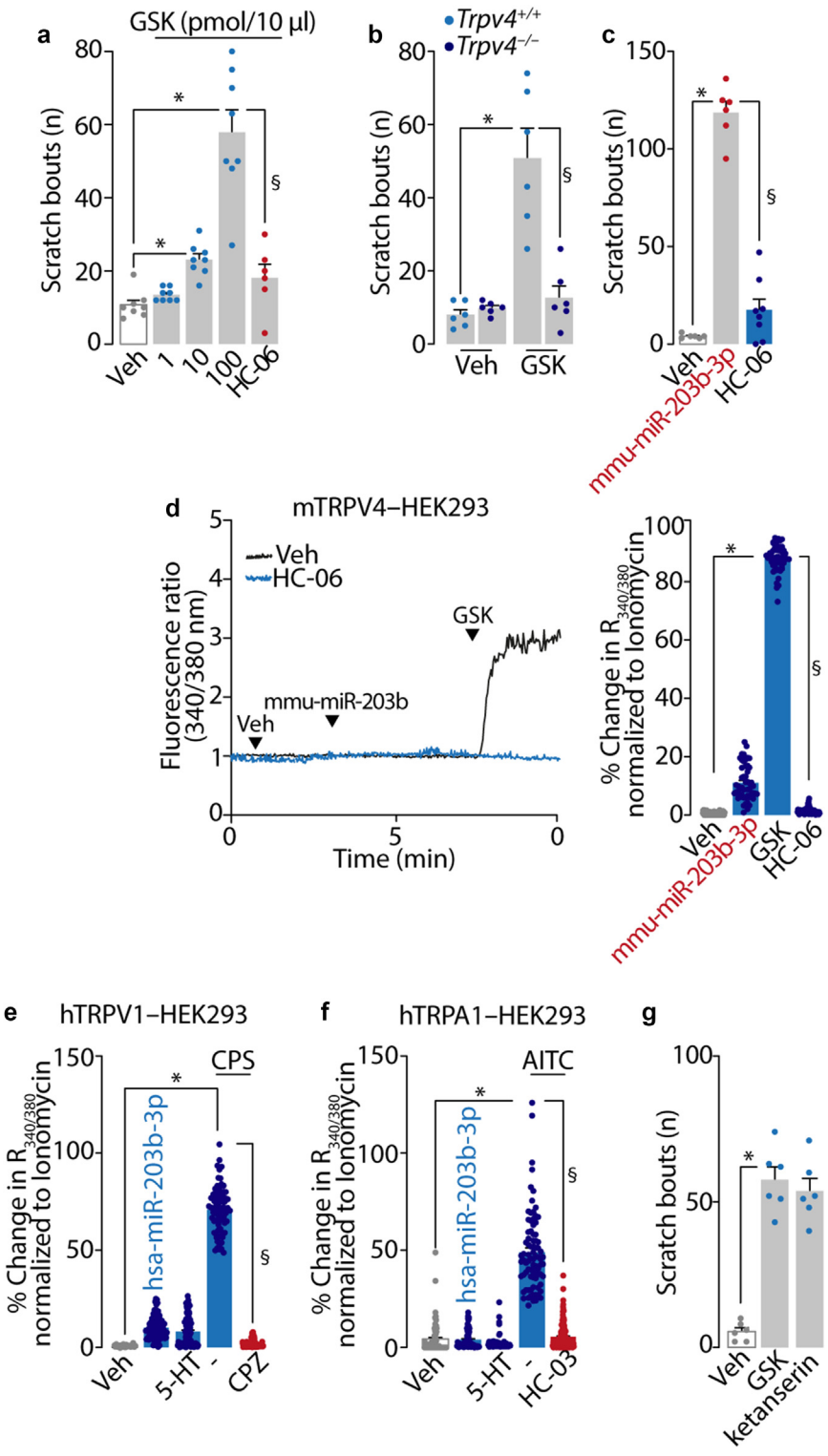

Supplementary Figure S1. miRNA-203b-3p evokes scratching behavior via TRPV4. (**a**) Dose-dependent scratching behavior in C57BL/6J mice induced by i.d. (10 µl) injection in the nape of the neck of GSK (1, 10, 100 pmol) or Veh and pretreated (0.5 hr) with HC-06 (10 mg/kg, i.p.) or Veh. (**b**) Scratching behavior in *Trpv4*$^{+/+}$and *Trpv4*$^{-/-}$ mice induced by GSK (100 pmol, i.d.) or Veh. (**c**) Scratching behavior in C57BL/6J mice induced by mmu-miR-203b-3p (1 nmol, i.d.) or Veh and pretreated (0.5 hr) with HC-06 (10 mg/kg, i.p.) or Veh. (**d**) Typical traces and cumulative data of the Ca^{2+} response in mTRPV4−HEK293 cells exposed to mmu-miR-203b-3p (10 µM) and GSK (10 nM) or Veh in the presence of HC-06 (30 µM) or Veh. (**e**) Ca^{2+} response in hTRPV1−HEK293 cells exposed to hsa-miR-203b-3p (10 µM), 5-HT (1.5 mM), CPS (1 µM), or Veh in the presence of CPZ (30 µM) or Veh. (**f**) Ca^{2+} response in hTRPA1−HEK293 cells exposed to hsa-miR-203b-3p (10 µM), 5-HT (1.5 mM), AITC (10 µM), or Veh in the presence of HC-03 (30 µM) or Veh (n = 4 independent experiments). (**g**) Scratching behavior in C57BL/6J mice induced by GSK (100 pmol, i.d.) or Veh and pretreated (0.5 hr) with ketanserin (1 mg/kg, i.p.) or Veh. (n = 6−8 mice per group). Dash (−) represents the combination of different Vehs. Data are presented as mean ± SEM. $^{*}P < 0.05$ versus Veh and $^{\S}P < 0.05$ versus GSK, mmu-miR-203b-3p, CPS, and AITC. Data were analyzed with one-way ANOVA with Bonferroni correction. 5-HT, serotonin; AITC, allyl isothiocyanate; Ca^{2+}, calcium ion; CPS, capsaicin; CPZ, capsazepine; GSK, GSK-1016790A; HC-03, HC-030031; HC-06, HC-067047; HEK293, human embryonic kidney 293; hr, hour; hTRPA, human TRPA1; hTRPV1, human TRPV1; i.d., intradermal; i.p., intraperitoneal; min, minute; mTRPV4, mouse TRPV4; Veh, vehicle.

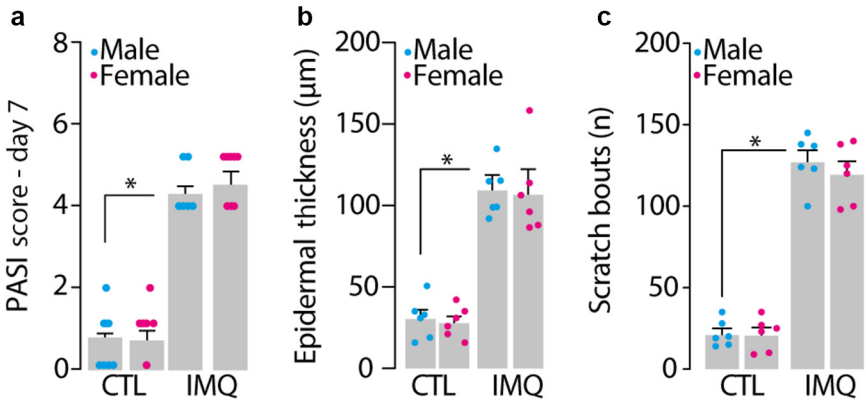

Supplementary Figure S2. PASI score, epidermal thickness, and scratching behavior in male and female mice. (**a**) Cumulative PASI score, (**b**) epidermal thickness, and (**c**) scratching behavior in C57BL/6J male and female mice on day 7 after IMQ or vehicle (CTL) treatment. (n = 6 mice per group). Data are presented as mean ± SEM. **P* < 0.05 versus CTL. Data were analyzed with one-way ANOVA with Bonferroni correction. CTL, control; IMQ, imiquimod.

Supplementary Table S1. Rat and Mouse Primers Used in this Study

Primers	Sequence (5′–3′)
Rat b-Actin (NM_031144)	F: CCGCGAGTACAACCTTCTTG
	R: ATACCCACCATCACACCCTG
Rat HTR1A (NM_012585)	F: AAAGAGCACCTTCCTCTG
	R: AGAGCCACAATGAAAAACG
Rat HTR1B (NM_022225)	F: AAAAGAACTCCCAAAAGGG
	R: AGGGTGGGTAAATAGAAAGC
Rat HTR1D (NM_012852)	F: AAAGCCACTAAGACATTGG
	R: CCACGTGAAGAAGTCAAAG
Rat HTR1F (NM_021857)	F: AAAATATACAGAGCAGCAAGG
	R: AACATGTAGGATGTGGAGAC
Rat HTR2A (NM_017254)	F: ATCTGTAGGTATATCCATGCC
	R: CACAAAAGAGCCTATGAGAAC
Rat HTR2B (NM_017250)	F: ACAATCATGTTTGAGGCTAC
	R: CTGAATTGGCTTTTTGATGG
Rat HTR2C (NM_012765)	F: GGGCAATATCAATAGGAGTTTC
	R: AGGACGTAGATCGTTAAGAAG
Rat HTR3A (NM_024394)	F: CCTCATTGGTGTCTACTTTG
	R: CTATTCTGTCTAGGACCAGG
Rat HTR3B (NM_022189)	F: CTCTTGATTCCTAGCATCTTC
	R: GTAAAGAAGACCCCAATCAG
Rat HTR4 (NM_012853)	F: ACTCATGTGCTAAGGGATAC
	R: CTTAGGACTGGCTTCTTTTC
Rat HTR5A (NM_013148)	F: CAAACTTCCATAACAGCCTC
	R: CTTTGATATGTTTGGGGACAG
Rat HTR6 (NM_024365)	F: AATGTTGCTTGTGTAGTGTG
	R: GACAGATTGCTTTCCTACTG
Rat HTR7 (NM_022938)	F: ATATATGCCTTCTTCAACCG
	R: GTGGTCAGAGTTTTGTCTTAC
Rat TRPV4 (NM_023970)	F: GTTTGAGGGAGAGGAAGGCT
	R: TCTACGACCTTCCTCCTCCA
Mouse b-Actin (NM_007393)	F: GACCTCTATGCCAACACAGT
	R: GGAGCAATGATCTTGATCTT
Mouse HTR1A (NM_008308)	F: CTCACCCTCAGTTTCTTTTC
	R: TCTAAGTCTCCAACCTCTTG
Mouse HTR1B (NM_010482)	F: ACCCTAGGGATCATTTTAGG
	R: ATGAGGGAGTTAAGATAGCC
Mouse HTR1D (NM_008309)	F: GAATATACAAACACCTCAGAGC
	R: GTGACCAAGACTCAAAGAATG
Mouse HTR1F (NM_008310)	F: CACCACGGTATTCATTTCTTC
	R: CATTCGGTTTAACAGTTCCTC
Mouse HTR2A (NM_172812)	F: ATGAAAAGGTTAGCTGTGTG
	R: CGCAATGTTAAAAGCATCAC
Mouse HTR2B (NM_008311)	F: AGCGTCTTCTGGAATCTAAG
	R: AAGCAAGTCATCTGCTTTAG
Mouse HTR2C (NM_008312)	F: GTCTGGATTTCACTAGATGTG
	R: GAAACTCCTATTGATATTGCCC
Mouse HTR3A (NM_001099644)	F: CTCATCAATGAGTTTGTGGAC
	R: GAAGTTGTAGATGTCAAGGC
Mouse HTR3B (NM_020274)	F: GTGCAAGAATTGTGTTCAAG
	R: AAAGAAGACCCCAATCAGAG
Mouse HTR4 (NM_008313)	F: GGCATAGTTGATGTGATAGAG
	R: CTTAGCAGTGACATAGATTCG
Mouse HTR5A (NM_008314)	F: TTATTCTGAGCCCAGTGAG
	R: ATTCTTCACCTCCACAGC
Mouse HTR6 (NM_021358)	F: CATCTCTCCAGGTCTCTTC
	R: GGGGATAGATGATAGGGTTC
Mouse HTR7 (NM_008315)	F: GTTTGTGCTACAAAACTGTG
	R: CTGTTCTGCATTACTTCTTCTC
Mouse TRPV4 (NM_022017)	F: ATGCTTATCGCCCTCATGGGTG
	R: CAGGGAAGGAACGCTCGATGTC

(*continued*)

Abbreviations: F, forward; R, reverse.

Supplementary Table S2. Binding-Free Energy Values Calculated for the Seven Most Stable miRNA–Protein Complexes Using the MM-PBSA Method

Complex	MM-PBSA Binding Energy (kcal/mol)
3	−13.2
5	−33.4
8	−32.3
10	−26.2
11	−78.5
13	−11.7
20	−42.0

Abbreviations: miRNA, microRNA; MM-PBSA, Molecular Mechanics Poisson–Boltzmann Surface Area.
Values are expressed in kcal/mol. This table is related to Figure 4.

Supplementary Table S3. Average RMSD Values of the miRNA Core Phosphorous Atoms during the Total 50 ns of MD Simulation Performed for the 11 Selected miRNA–Protein Complexes

Complex	miRNA RMSD
2	8.2
3	5.9
5	5.5
8	5.5
10	5.7
11	4.4
12	6.5
13	5.9
15	8.6
18	6.5
20	5.7

Abbreviations: MD, molecular dynamics; miRNA, microRNA; RMSD, root mean square deviation.
This table is related to Figure 4.

Supplementary Table S4. Average RMSD Values of the miRNA Core Phosphorous Atoms during the 25 ns of MD Simulation Initially Performed for the 22 miRNA–Protein Complexes

Complex	miRNA RMSD
1	8.6
2	5.1
3	5.7
4	7.7
5	5.4
6	11.4
7	6.7
8	5.2
9	17.0
10	5.8
11	5.0
12	5.8
13	5.4
14	6.4
15	5.7
16	12.5
17	7.3
18	4.9
19	6.6
20	5.4
21	6.7
22	7.7

Abbreviations: MD, molecular dynamics; miRNA, microRNA; RMSD, root mean square deviation.